Rs_MEP1 is required for the pathogenesis of *Rhizoctonia solani* AG1-IA in plants

Amrita Pradhan[1], Debashis Sahoo[1], Vikrant Bhati[2], Rahul Kumar[1], Rajni Yadav[1], Srayan Ghosh[1], Prashant Anupama-Mohan Pawar[2] and Gopaljee Jha[1], *

[1]BRIC-National Institute of Plant Genome Research, Aruna Asaf Ali Marg, New Delhi-110067, India

[2]Regional Centre for Biotechnology, Faridabad Rd, Faridabad, Haryana 121004

* To whom correspondence should be addressed

Corresponding author information:

Gopaljee Jha, PhD

Email: jmsgopal@nipgr.ac.in; jmsgopal@gmail.com

Tel: +91(0)1126735177

Fax: +91(0)1126741658

Abstract

Rhizoctonia solani AGI-IA is a polyphagous necrotrophic fungal pathogen that causes sheath blight disease in rice. Efforts are being made to identify pathogenicity-associated genes in *R. solani* and modulate them to develop a disease control strategy. Here, we investigate the roles of some predicted pathogenicity-associated genes of *R. solani* that have previously been reported to be upregulated during infection in rice. The tobacco rattle virus-based host-induced gene silencing of the selected pathogenicity-associated genes revealed that silencing of *Rs_MEP1*, a zinc-containing Peptidase_M43 domain-metalloprotease, severely compromises *R. solani* infection in tomato. Moreover, double-stranded RNA-mediated silencing of *Rs_MEP1* prevented *R. solani* infection in rice. The signal sequence trap assay indicated the secretory nature of Rs_MEP1, while the reporter assay suggested its localization in the plant apoplast. Notably, agrobacterium-mediated transient overexpression of Rs_MEP1 induces necrotic cell death responses in plants. We provide evidence that *Rs_MEP1* interacts with GH19 family of rice chitinases and potentially modulates their functions. Overall, our study emphasizes that *Rs_MEP1* facilitates *R. solani* in promoting necrotic responses and targets rice GH19 chitinases to impart disease susceptibility in plants.

Keywords: Cell wall degrading enzyme, Chitinase, Effector, HIGS, Metalloproteases, Necrotroph, Sheath blight disease

Introduction

Rhizoctonia solani is one of the highly destructive polyphagous fungal pathogens that causes sheath blight disease, leading to ~50% yield reduction in rice (Molla et al. 2020; Pradhan et al. 2021; Singh et al. 2019). Several QTLs (quantitative trait loci) are reported to be associated with sheath blight disease resistance in rice (Liu et al. 2024; Feng et al. 2025; Wang et al. 2021). However, their adoption in resistant breeding programs has been limited. Therefore, understanding the intricacies of rice-*Rhizoctonia* interactions has been a focus area of research, and the findings from such studies have implications in developing disease control strategies.

During plant-fungus interactions, the apoplast serves as a prime battleground, wherein the plant deploys pattern-recognition receptors to surveil potential pathogens and trigger defense responses (Rocafort et al. 2020). Also, being enriched in hydrolytic enzymes, antimicrobial secondary metabolites, and proteases, the apoplast provides a hostile environment for the pathogen's growth. On the other hand, fungal pathogens deploy specialized effector proteins in the apoplast to evade host surveillance and impede elaboration of plant defense responses. Upon pathogen perceptions, one of the conserved plant responses is to upregulate various chitinases that hydrolyze chitin, a major constituent of the fungal cell wall, and induce chitin-triggered immunity (Pradhan et al. 2021; Gong et al. 2020; Martínez-Cruz et al. 2021; Rocafort et al. 2020). However, as a counter-defense strategy, the pathogens deploy effectors to prevent the elaboration of defense responses. For example, *Cladosporium fulvum* utilizes Avr4 (CBM14, carbohydrate-binding module family 14) to prevent maize chitinases from hydrolyzing its chitinaceous cell wall (van den Burg et al. 2006). *C. fulvum* utilizes conserved LysM, lysin motif-containing effector Ecp6 (CBM family 50) to sequester chitin oligosaccharides and prevent chitin-triggered immunity in plants (de Jonge et al. 2010). *Moniliophthora perniciosa* produces a catalytically inactive chitinase that binds to and sequesters chitin oligomers to suppress immune responses during infection in Cacao (Fiorin et al. 2018). Moreover, some pathogens, including *Ustilago maydis,* can directly degrade host chitinases by utilizing fungalysin M36 metalloproteases, as effector proteins (Ökmen et al. 2018; Sanz-Martín et al. 2016). Understanding how *R. solani* tackles host immune responses during plant colonization remains largely unknown.

The genome analysis, comparative genomics, and interaction transcriptomics have identified potential pathogenicity factors, including secreted effectors of *R. solani* (Francis et al. 2023; Ghosh et al. 2019; Hane et al. 2014; Lee et al. 2021; Wibberg et al. 2016; Zheng et al. 2013a).

Some of these proteins are anticipated to modulate plant responses and create a conducive environment that facilitates pathogen colonization in the host (Tariqjaveed et al. 2021; Pradhan et al. 2021). For example, Rs_CRZ1, a calcineurin-responsive zinc-finger transcription factor (Ghosh et al. 2021), and Rs_MET13, a gene involved in methionine biosynthesis (Das et al. 2024), facilitate *R. solani* infection in plants. RsIA_Peptidase_S8 and RsIA_GT (glycosyltransferase) effector proteins of *R. solani* are involved in inducing host cell death (Niu et al. 2021; Zheng et al. 2013b). Moreover, RsIA_CtaG/Cox11, the mitochondrial-targeting effectors of *R. solani,* are potentially involved in suppressing the host immune responses (Zhang et al. 2024).

In the present study, we endeavored to identify and characterize key pathogenicity-associated genes of *R. solani* that are upregulated during colonization in rice. We report that a zinc-containing Peptidase_M43 domain-containing secreted metalloprotease, *Rs_MEP1* (*R. solani metalloprotease 1*), is important for disease establishment in rice and tomato. We present evidence that Rs_MEP1 is potentially localized in the apoplast and it interferes with the activity of host chitinases. Our data support the notion that Rs_MEP1 is an important pathogenicity determinant of *R. solani* and a novel target for controlling sheath blight disease in rice. It is to be noted that fungal Peptidase M43 proteins are structurally as well as functionally different from endogenous zinc-dependent metalloproteases of plants (Morimoto et al. 2022; Pan et al. 2020). Our study exemplifies the evolutionary adaptation of fungal pathogens to utilize metalloproteases as apoplastic effectors to target host functions to promote disease susceptibility.

Results

Silencing of candidate pathogenicity determinants compromises *R. solani*'s ability to infect plants

In a previous transcriptome-based study, we identified certain proteases, transcription factors, sugar transporters, secreted effectors, and carbohydrate-active enzymes (CAZYmes) of *R. solani* that are upregulated during infection in rice (Ghosh et al. 2018). We selected some of them (Table S1) and followed a previously standardized Tobacco Rattle Virus (TRV) based host-induced gene silencing (HIGS) approach to effectively silence them and investigate their importance during infection in tomato, an alternate host of *R. solani* (Kant et al. 2019; Rani and Jha 2021; Ghosh et al. 2021). The silencing of *PDS* (phytoene desaturase) was used as a

positive control for VIGS, as the emerging leaves of pTRV: PDS-infiltrated tomato plants exhibited a photobleaching phenotype (Fig. S1A). Among various tested genes, silencing of *Rs_ABC* (*R. solani ATP-binding cassette transporter*) and *Rs_MEP1* (*R. solani* metalloprotease 1) genes significantly compromised *R. solani* infection in tomato (Fig. S1). Notably, silencing of *Rs_MEP1* had a more pronounced effect, leading to a significant reduction in necrotic symptoms (Fig. S1A) and disease severity index in tomato (Fig. S1B). On the other hand, as reported previously (Ghosh et al. 2021), silencing of *Rs_GT34* (*R. solani* glycosyl transferase family 34 protein) did not prevent *R. solani* infection in tomato.

Rs_MEP1 is a conserved secreted effector protein of *R. solani*

BlastP searches of the UniProt database and Clustal Omega analysis revealed that Rs_MEP1 shows significant homology with extracellular metalloproteases from various fungi. It harbours a Peptidase_M43/ZnMc_pappalysin-like domain containing a HEXXH active site motif, typical of zinc metalloproteases (Fig. 1A, Fig. S2A). Structure modelling using I-TASSER server (Zhou et al. 2022) reflected that Rs_MEP1 (without signal peptide) has structural analogy with Promirolysin (6R7V), a previously reported metalloprotease (Fig. S2B). Blast searches revealed that Rs_MEP1 homologs are present in *R. solani* strains belonging to AG-1 IA, AG-1 IB, AG-3, AG-8 anastomosis groups, but absent in AG-2, AG-4, and AG-5 strains (Table S2).

SignalP (Nielsen et al. 2024) search revealed that Rs_MEP1 contains an N-terminal signal peptide (SP; signal peptide likelihood: 0.9651). We performed a signal sequence trap assay in yeast to support the secretory nature of the protein (Lee et al. 2006; Singh et al. 2023). For this, the coding sequence of Rs_MEP1 (with and without SP) was fused with the invertase (SUC2) of *S. cerevisiae* (yeast) that lacked SP, in pYST vector, and transformed into *suc2* mutant strain of yeast. The yeast cells expressing full-length Rs_MEP1 were able to grow on sucrose-supplemented plates, whereas those expressing Rs_MEP1 without SP (Rs_MEP1ΔSP) or vector control failed to grow on such plates (Fig. 1B, C). The analysis suggested that Rs_MEP1 has a functional signal peptide that may facilitate protein secretion during fungal colonization of plants.

EffectorP (Sperschneider and Dodds 2022) search indicated an apoplastic localization of Rs_MEP1. To test this, we created a GFP fusion construct of Rs-MEP1 (with and without SP) in the pCAMBIA1302 binary vector. Rs_MEP1:GFP/ Rs_MEP1ΔSP:GFP fusion proteins and mCherry-tagged apoplast marker, pCMU-APr (Ivanov and Harrison 2014), were co-expressed

in *Nicotiana benthamiana* leaves using Agrobacterium-mediated transformation. The confocal microscopy revealed that in the case of full-length Rs_MEP1, the reporter GFP signal is co-localized with the RFP signal of the apoplast marker (Fig. 1D). On the other hand, in the case of signal peptide-deleted Rs_MEP1 (Rs_MEP1ΔSP:GFP), the GFP signal was not co-localized with the RFP signal. Overall, our data support the apoplastic localization of Rs_MEP1.

***Rs_MEP1* is important for *R. solani* infection in plants**

It is to be noted that *Rs_MEP1* was significantly upregulated during 48-72 h (maximum upregulation was observed at 60 h) of *R. solani* infection in tomato (Fig. S3A). The gene expression was significantly reduced in the *Rs_MEP1*-silenced (pTRV: *Rs_MEP1*-infiltrated) plants, compared to the vector control (pTRV:*0*-infiltrated) plants (Fig. S3 B). We observed the *Rs_MEP1*-silenced plants to have reduced ROS (reactive oxygen species) accumulation (DAB, 3,3′-Diaminobenzidine staining) and cell death (Trypan blue staining) under *R. solani* infected conditions (Fig. S3C). The disease index (Fig. S3D) and pathogen load (Fig. S3E) were also significantly reduced in *Rs_MEP1*-silenced plants. Further, we used WGA-FITC staining to examine the colonization pattern of *R. solani* and observed that the formation of the infection cushion was significantly compromised in *Rs_MEP1*-silenced plants compared with vector control and wild-type (WT) plants (Fig. S4 A, B). Similarly, three-dimensional (3D) topological imaging revealed a thick mat of mycelial invasion in *R. solani*-infected WT and vector control plants. In contrast, only limited fungal proliferation was observed in *Rs_MEP1*-silenced plants. Deep penetration of *R. solani* mycelia was observed in WT (~43 μM) and vector control (~30 μM) plants, whereas *Rs_MEP1*-silenced plants had significantly reduced penetration (penetration depth ~18 μm) (Fig. S4 C, D).

We also adopted the dsRNA-mediated silencing approach as standardized previously (Gebremichael et al. 2021; Ghosh et al. 2021; Francis et al. 2023), to silence and investigate the importance of *Rs_MEP1* in facilitating *R. solani* infection. We synthesized *Rs_MEP1*-specific dsRNA and observed that it effectively knocked down *Rs_MEP1* expression during infection in tomato (Fig. S5A). The disease symptoms (Fig. S5B), disease severity index (Fig. S5C), and pathogen load (Fig. S5D) were significantly reduced in *Rs_MEP1*_dsRNA-treated *R. solani* sclerotia, compared to those treated with buffer. Silencing of *Rs_GT34* did not compromise *R. solani* pathogenesis in tomato.

To investigate further, we generated transgenic *Arabidopsis* lines (n=4) expressing the RNAi construct against *Rs_MEP1* (Figure S6A) and propagated them to T2 generation. The

expression of *Rs_MEP1* (normalized using Arabidopsis *actin* gene) was significantly downregulated in RNAi lines under infected conditions (Fig. S6B). Notably, RNAi lines exhibited significantly reduced disease symptoms, including cell death (Fig. S6C), and disease index (Fig. S6D), compared to vector control and WT plants, at 4 dpi of *R. solani* infection.

Collectively, these analyses highlighted the importance of Rs_MEP1 in driving *R. solani* pathogenesis in plants.

The dsRNA-mediated silencing of *Rs_MEP1* compromises *R. solani* infection in rice

After establishing the role of *Rs_MEP1* in *R. solani* infection in tomato and Arabidopsis, we investigated its function during sheath blight disease development in rice. We used dsRNA-mediated gene silencing and observed that treating rice with *Rs_MEP1*-specific dsRNA effectively reduced *Rs_MEP1* expression in infected sheaths (Fig. 2A). Moreover, *Rs_MEP1*-silenced (dsRNA-treated) sclerotia were compromised in establishing disease in rice. Significantly reduced disease symptoms as well as ROS accumulation (Fig. 2B), lower relative vertical sheath colonization (RVSC) disease index (Fig. 2C), and reduced pathogen load (Fig. 2D) were observed in rice sheaths infected with *Rs_MEP1*-silenced sclerotia, compared to those infected with wild-type (WT) sclerotia. On the other hand, *Rs_GT34*-silenced sclerotia were proficient in establishing disease. WGA-FITC staining revealed that the fungal biomass was significantly reduced in rice infected with *Rs_MEP1*-silenced sclerotia compared to those infected with *Rs_GT34*-silenced and WT sclerotia (Fig. 2E). Additionally, three-dimensional (3D) topological imaging showed a thick mat of mycelial invasion in WT and *Rs_GT34*-silenced plants. In contrast, only limited fungal proliferation was observed in plants infected with *Rs_MEP1*-silenced sclerotia (Fig. 2F). Compared to WT (~38 µm) and *Rs_GT34*-silenced (~35 µm), *Rs_MEP1*-silenced (~18 µm) plants had significantly reduced penetration of *R. solani* mycelia (Fig. 2G). These analyses suggest that Rs_MEP1 is important for host colonization.

Heterologous overexpression of Rs_MEP1 induces cell death in plants

Further, we used an Agrobacterium-mediated transient overexpression system to analyze the effect of Rs_MEP1 on rice and *Nicotiana benthamiana* leaves. We observed that heterologous expression of *Rs_MEP1* induced necrotic symptoms in infiltrated regions at 5 dpi, whereas infiltration with the vector control did not induce necrosis (Fig. 3A and B). Moreover, H_2DCFDA staining reflected that *Rs_MEP1*-infiltrated regions had a higher level of ROS accumulation, compared to the vector control plants (Fig. 3C). Immunoblot analysis using anti-

His antibody reflected that Rs_MEP1 is expressed in leaves with necrotic symptoms (Fig. 3D). Considering the above, we speculate that Rs_MEP1 is important for inducing cell death response during *R. solani* infection in plants.

_Rs_MEP1_ interacts with a rice chitinase protein

Phytopathogenic fungal metalloproteases have been shown to target host chitinases and suppress the elaboration of plant defense responses (Ökmen et al. 2018). In previously reported transcriptome (RNAseq) data (Ghosh et al. 2017), we observed that several rice chitinase genes were upregulated during *R. solani* infection in rice (Table S3). The qRT-PCR revealed that the expression of chitinase encoding genes (*Os_02g39330*, *Os_04g41680*, *Os_04g28080*, *Os_04g51060*, and *Os_04g51050*) are upregulated in infected rice, at 3 dpi and 4 dpi (Fig. 4A). We selected Os_04g41680, belonging to CBD (chitin-binding domain) containing GH19 family of chitinases, and Os_04g28080 which lacks CBD (belonging to GH18 family) to study the physical interaction with Rs_MEP1 using yeast two-hybrid assay. The Rs_MEP1 was cloned into pGADT7 (as a fusion protein with Gal4 activation domain), and chitinases (Os_04g41680/ Os_04g28080) were cloned into pGBKT7 (as a fusion protein with Gal4 DNA-binding domain). The yeast cells transformed with pGADT7:Rs_MEP1 and pGBKT7:Os_04g41680 showed growth on Synthetic Dropout (SD) medium lacking histidine and adenine. On the other hand, yeast cells transformed with pGADT7:Rs_MEP1 and pGBKT7:Os_04g28080, or empty vector, were unable to grow on the plate. This indicated that Rs_MEP1 and rice chitinase (Os_04g41680) demonstrate physical interactions (Fig. 4B).

We also investigated the interaction between Rs_MEP1 and Os_04g41680 under in-planta conditions using bimolecular fluorescence complementation (BiFC) assays. In BiFC assay, the reconstitution of YFP fluorescence was observed in *N. benthamiana* leaves that co-express Rs_MEP1 and rice chitinase proteins, while in the case of vector control, no signal was observed (Fig. 4C). Notably, the YFP signal merged with the RFP signal of the apoplastic marker, pCMU-APr (Ivanov and Harrison 2014). Taken together, our data suggest that Rs_MEP1 interacts with Os_04g41680 during plant colonization by *R. solani*.

Further, we attempted to overexpress and purify Rs_MEP1 protein from *E. coli*. However, we had difficulty inducing the protein and reproducibly obtaining it in the soluble fraction. We realized that, as a secreted fungal effector protein, expressing and purifying Rs_MEP1 in *E. coli* may not be ideal, as it does not address post-translational modifications such as glycosylation, which might influence the protein's activity. With extensive standardization, in

a few protein preparations, we obtained Rs_MEP1 protein in the soluble fraction and further assessed its effect on chitinase activity using a commercially available Fluorimetric Kit (Sigma Aldrich). Our data showed that Rs_MEP1 significantly reduced the activity of the chitinase (provided in the kit) from 5.07 Units/ml to 3.42 Units/ml (Fig. 4D). We also tested the inhibitory activity of Rs_MEP1 on rice chitinase (Os_04g41680). For this, we cloned the genes (*Rs_MEP1* and *Os_04g41680*) into a T-DNA binary vector and transiently expressed the proteins in *N. benthamina* leaves, using agroinfiltration. Chitinase activity was evaluated using crude protein extracts prepared from samples collected at different time points. Notably, Rs_MEP1 inhibited the chitinase activity of Os_04g41680 (Fig. 4E).

We also tested whether Rs_MEP1 can inhibit the activity of other cell wall-degrading enzymes. We observed that in the presence of an equal concentration of xylanase and Rs_MEP1 (1:1), there was no significant difference in the xylose release (Fig. 5A). However, with an increase in the proportion of Rs_MEP1 (1:10 and 1:15), there was a significant decrease in xylose release from acetylated xylan (Fig. 5B). The ratio 1:10 and 1:15 showed 15% and 11% decrease in xylose release in the presence of Rs_MEP, suggesting significant inhibition of xylanase activity. We also performed the xylanase inhibition assay using Arabidopsis cell wall powder (which mimics in vivo condition) as a substrate of xylanase and observed that xylose release was reduced by 10% in the presence of Rs_MEP1, as compared to individual xylanase treatment (Fig. 5C). Moreover, we tested the inhibitory effect of Rs_MEP1 on a cocktail of cell wall degrading enzymes (CTec2) using extracted Arabidopsis cell wall powder as substrate and estimated release of glucose. The glucose release was reduced by 13-14% when CTec2 was incubated with Rs_MEP1, as compared to individual treatment (Fig. 5D). This suggests that multiple enzymes involved in cellulose hydrolysis might be inhibited by Rs_MEP1. Considering the above, we propose that Rs_MEP1 possesses broad-spectrum inhibitory activity against various cell wall–degrading enzymes. The relevance of such broad-spectrum cell wall–degrading enzymes inhibition activity of Rs_MEP1 in promoting *R. solani* infection has to be further investigated.

Discussion

Understanding the mechanism by which *Rhizoctonia solani*, the causal agent of rice sheath blight disease, infects a wide range of plant species is important for developing control strategies. In this study, we explored the involvement of candidate pathogenicity determinants

(*Rs_MEP1, Rs_GT34, Rs_AOX1, Rs_GzZC36, Rs_GAS1, Rs_GST, Rs_ABC3, Rs_PHO84, and Rs_SPM1*) that are upregulated during *R. solani* infection in rice (Ghosh et al. 2018). As the genetic transformation of *R. solani* remains challenging, we set up a virus-induced gene silencing (VIGS)-based HIGS (host-induced gene silencing) approach to silence selected candidate pathogenicity determinants during infection in tomato. Amongst the tested genes, silencing of *Rs_MEP1*, an M43-domain-containing metalloprotease, had severely compromised the pathogen's ability to cause disease. Infection cushion formation and penetration into host tissues are important features for successful host colonization of *R. solani* (Ghosh et al. 2021; Senapati et al. 2022). We observed that these features were compromised upon silencing of *Rs_MEP1*. To support the role of *Rs_MEP1* in promoting *R. solani* pathogenesis, we developed stable RNAi lines in *A. thaliana* and observed that the transgenic lines were highly tolerant to *R. solani* infection. Furthermore, using dsRNA-mediated gene silencing, we demonstrated that *Rs_MEP1* is important for the establishment of sheath blight disease in rice.

The *in-silico* analysis, yeast secretion trap assay, and localization study in *N. benthamiana* supported the apoplastic localization of Rs_MEP1. The M43-type secreted metalloproteases appear to be largely fungal/bacterial in origin and lack clear homologs in tomato or rice. This strengthens our argument that Rs_MEP1 is a pathogen-specific effector. Previously, the M43-domain-containing metalloprotease of *Rhizoctonia cerealis* (RcMEP1) had been shown to elicit cell death in *N. benthamina* leaves (Pan et al. 2020). We also observed that agrobacterium-mediated transient overexpression of Rs_MEP1 enhanced ROS production and triggered cell death (necrosis-like symptoms) in rice and *N. benthamiana* leaves. We reasoned that the effector-like metalloprotease activity of Rs_MEP1 could degrade various host proteins. Indeed, several rice chitinases are upregulated during *R. solani* infection in rice (Ghosh et al. 2017). The Y2H and BiFC assays revealed that Rs_MEP1 interacts with the CBD-containing rice chitinase, Os_04g41680, but not with Os_04g28080, which lacks the CBD domain. Our data suggest that Rs_MEP1 inhibits the activity of chitinase and other cell wall-degrading enzymes, including xylanase and cellulase (Fig. 6). Akin to previously reported fungal metalloproteases (UmFly1 of *Ustilago maydis*), we speculate that Rs_MEP1 enables *R. solani* to suppress chitin-triggered immunity during host colonization. Also, because of Rs_MEP1's inhibitory action on xylanase and cellulase, it may alter the milieu of cellulose- and xylan-derived oligosaccharides, thereby affecting the oligosaccharide-mediated immune response (Dewangan et al. 2023).

Growing evidence suggests that fungal pathogens have evolved metalloproteases that are structurally and functionally distinct from plants' endogenous metalloproteases, as apoplastic effectors to target host chitinases (Pan et al. 2020; Ökmen et al. 2018; Sanz-Martín et al. 2016; Jashni et al. 2015; Naumann et al. 2011). Rs_MEP1 of *R. solani* is one such example; the pathogen deploys it to target host chitinases during colonization. Developing biotechnological interventions to target these effectors may enable plants to elicit chitin-triggered immunity upon pathogen perception and combat them. This is supported by our observation that dsRNA-mediated silencing of Rs_MEP1 effectively controls sheath blight disease in rice. We propose that designing novel variants of enzymatically active chitinase proteins that cannot be targeted by fungal metalloproteases (potentially by deleting their metalloprotease-binding sites) will facilitate to strengthen host immune responses against phytopathogenic fungi.

Materials and Methods

Biological materials and growth conditions

The sclerotia of *Rhizoctonia solani* AG1-IA (BRS1 strain) were grown on potato dextrose agar (PDA) [Himedia, India] plates at 28 ^{0}C (Francis et al. 2023; Ghosh et al. 2014). *Escherichia coli* strains were grown on LBA (Luria-Bertani Agar media; Himedia, India) at 37 ^{0}C. Agrobacterial strains were grown on YEP (Yeast Extract Peptone; Himedia India) agar plates at 28^{0}C. *Saccharomyces cerevisiae* was grown on YPD (1% yeast extract, 2% peptone, 2% glucose, Himedia) agar plates, at 28 ^{0}C. Rice (*Oryza sativa* ssp. *indica* 'PB1') and tomato (*Solanum lycopersicum* cultivar 'Pusa Ruby') plants were grown under greenhouse conditions at 28 ^{0}C temperature, 80% relative humidity (RH) and 12/12 h (day/night) and 26 ^{0}C temperature, 65% RH and 16/8 h (day/night) conditions, respectively.

R. solani infection in tomato

The leaves of three-week-old tomato (cv. PB1) plants were infected with *R. solani* sclerotia and incubated in growth chambers at 28 ^{0}C and 80% RH, as described in (Kant et al. 2019; Rani and Jha 2021). A minimum of 10 plants with at least three leaves per plant were infected with *R. solani* in each experiment, and at least three independent experiments were conducted. The appearance of disease symptoms was monitored, as described in (Francis et al. 2023), and categorized into severe (total necrosis with coalescence of several necrotic spots, >30% of infected region of the leaves showing necrotic lesions), mild (localized necrotic spots, <30%

of infected region of the leaves showing necrotic lesions), and no symptoms (visible necrotic symptoms not observed). The samples were collected at different time points (0 h, 12 h, 24 h, 48 h, and 72 h) for further analysis.

***R. solani* infection in rice**

The sclerotia were placed in the sheath of rice (*Oryza sativa* L. cv. PB1) tillers (45 days old) using sterile forceps, as described earlier (Francis et al. 2023). The progression of disease symptoms was monitored. The distance between the tips of the lowest and highest lesions of the infected sheath was measured as vertical sheath colonization (VSC) (Willocquet et al. 2011; Ghosh et al. 2017). The relative vertical sheath colonization (RVSC) was calculated by the formula VSC/sheath length X 100 as described before (Jia et al. 2013). At least 15 rice sheaths per treatment were examined in each experiment, and experiments were independently repeated three times. The infected tissues were harvested at different time intervals for further analysis.

Quantification of infection depth

R. solani-infected leaf (tomato)/ sheath (rice) samples were harvested at 3 dpi. For confocal microscopic analysis, the samples were cut into small pieces and autoclaved in 1 mM KOH (potassium hydroxide; Amresco), as described earlier (Ayliffe et al. 2013; Ghosh et al. 2021). Upon incubation in 50 mM Tris (pH 7.0) buffer for 15-20 min (used for pH neutralization), the samples were stained with WGA-FITC solution (20 µg/ml; Sigma Aldrich) for 20-30 min (under dark) (Ghosh et al. 2021). Upon gentle washing with sterile MQ water, samples were analyzed under green fluorescent protein (GFP) filter of the confocal laser scanning microscope (Leica AOBS TCS-SP5). The images were analyzed using LAS AF version 2.6.0 build 7266, and a topological 3D image was created to reflect the depth of pathogen penetration. The areas of the infection cushions were measured using ImageJ (http://rsbweb.nih.gov/ij) software, as described by (Ghosh et al. 2021). The experiment was performed with three independent biological replicates, with at least ten leaves analyzed in each replicate.

Histochemical assays in rice and tomato

Diaminobenzidine (DAB) staining

ROS accumulation in the *R. solani*-infected tissues was visualized by the DAB (3,39-diaminobenzidine) staining, as described earlier (Ghosh et al. 2017). Briefly, the infected samples were harvested and stained overnight in 1 mg/ml DAB solution (prepared in 50 mM

Tris-acetate buffer, pH 5.0) with gentle shaking in the dark. Upon washing with distilled water, samples were destained in a solution of ethanol/ glacial acetic acid (3:1 ratio) for 3-4 h. ROS accumulation was visualized as brown-colored patches and photographed using a Nikon D5600 DSLR camera. The experiment was independently repeated three times, and a minimum of three leaves (for tomato)/ sheath (for rice) per plant were analyzed in each experiment.

H_2DCFDA Staining

The H_2DCFDA (2',7'-Dichlorodihydrofluorescein diacetate) staining was also used to visualized the ROS accumulation (Sahoo et al. 2026). For this the H_2DCFDA solution (5 µmol/L) was prepared in milli Q water (Kuběnová et al. 2023). The harvested plant tissues were incubated in H_2DCFDA solution 30-45 minutes at room temperature under dark conditions. Upon brief washing, samples were analyzed under the green fluorescent protein (GFP) filter of a confocal laser scanning microscope (Leica AOBS TCS-SP5).

Trypan blue staining

Trypan blue staining of the infected samples was used to estimate the extent of host cell death (Ghosh et al. 2017). Briefly, samples were stained in 0.02% trypan blue solution (Himedia, India) overnight with gentle shaking. Upon incubation for 3-4 h in a destaining solution (ethanol: glacial acetic acid, 3:1, v/v), and gentle washing with distilled water, the appearance of blue colour (indicating host cell death) was monitored and photographed with a Nikon D5600 DSLR camera. The experiment was independently repeated three times, and a minimum of three leaves/ sheaths of infected plants were analyzed in each experiment.

RNA Isolation, cDNA synthesis, and qRT-PCR-based expression studies

The 4-5 excised leaves/ sheaths were pooled and used for total RNA isolation using RNAeasy Plant mini kit (Qiagen, Germany). 1 µg of RNA was used for cDNA synthesis using Verso cDNA Synthesis Kit (Thermo Fisher Scientific, USA). qRT-PCR-based gene expression analysis was performed using gene-specific primer pairs and Power Up SYBR Green master mix (Applied Biosystems) using 7900HT Real-Time PCR instrument (Thermo Fisher Scientific, USA). The relative gene expression was calculated using $2^{-\Delta Ct}$ method (Ct; cycle threshold) as described in (Kant et al. 2019). Fold change was estimated by $2^{-\Delta\Delta Ct}$ method (Livak and Schmittgen 2001), as described in (Chandan et al. 2023a). List of primers used in this study is listed in Table S4. Each experiment was repeated three times, with three technical and three biological replicates.

Estimation of Pathogen Load

Pathogen load in the infected samples was estimated by qRT-PCR as an abundance of *18S rRNA* of *R. solani* using the $2^{-\Delta Ct}$ method, as described in (Ghosh et al. 2021). ΔCt is the difference between Ct values of *18S rRNA* of *R. solani* (as target) and endogenous host genes (rice, *18S*; tomato, *actin;* and Arabidopsis, *actin*).

Construction of HIGS vectors to silence *R. solani* genes

The host-induced gene silencing (HIGS) approach was used to silence *R. solani* genes, as described in (Ghosh et al. 2021). The sequence of the target genes was analyzed using siFi21 software (http://labtools.ipk-gatersleben.de/) (Lück et al. 2019) and a unique gene fragment with no off-target silencing effect in *R. solani* and in tomato was selected. The gene fragments were PCR-amplified from *R. solani* genomic DNA, using gene-specific primer pairs (Table S4) that included suitable restriction sites. After sequence confirmation, the fragments were cloned into the pTRV2 vector using restriction enzymes. Upon confirmation by restriction digestion and Sanger sequencing, the positive constructs (recombinant pTRV2) and pTRV1 were mobilized into *Agrobacterium tumefaciens* (GV3101). PDS (phytoene desaturase; NM_001247166.2) gene, encoding an essential plant carotenoid biosynthetic enzyme, was used as a positive control for gene silencing.

A. tumefaciens strains harboring pTRV1, pTRV2, and recombinant pTRV2 vectors were grown in Yeast extract Broth (YEB) medium supplemented with rifampicin (50mg/ml) and kanamycin (50 mg/ml) at 28 ^{0}C overnight, under 200 rpm shaking conditions. The bacterial cells were harvested at 3000 rpm for 5 min (TOMY centrifuge CAX 571), and the pellet was resuspended in induction buffer [10 mM MgCl2, 10 mM MES (morpholine ethane sulfonic acid), and 200 µM acetosyringone]. The cultures (OD_{600}: 0.8) of pTRV2 (pTRV:Rs_MEP1) and pTRV1 (used as a helper virus) expressing Agrobacterium strains were mixed in a 1:1 ratio and infiltrated into the abaxial surface of 2-week-old tomato leaves using 1-ml needleless syringe (Kant *et al.*, 2019). The plants were incubated at 26 ^{0}C, under 16-h/8-h day/night conditions with 80% relative humidity. After 20 dpi (day post inoculum), the target gene silencing and plant phenotype were evaluated. The recombinant pTRV:PDS-infiltrated plants exhibited a photo-bleaching phenotype in developing leaves. The experiment was independently repeated three times, and a minimum of 15 leaves per plant were analyzed in each experiment.

Generation of RNAi construct

The gene fragment (356 bp) of *Rs_MEP1,* having no off-target silencing effect, was identified using siRNA-Finder (si-Fi) (http://labtools.ipk-gatersleben.de/) (Lück et al. 2019). The sense, as well as antisense fragments of *Rs_MEP1* were PCR amplified from *R. solani* cDNA using gene-specific primers and cloned into a modified pGEM-T Easy vector (having an intron sequence of *Brassica)*. The sense-intron-antisense cassette was sub-cloned into the pBI121 binary vector at XbaI/SacI sites to generate a hairpin RNAi construct (pBI121: Rs_MEP1). The construct was mobilized into Agrobacterium strains GV3101 for transformation in Arabidopsis plants. The floral dipping method was used for Arabidopsis transformation (Clough and Bent 1998; Chandan et al. 2023b). Kanamycin-resistant seedlings were selected for further confirmation. The positive transformants were confirmed using gene-specific primers and kanamycin primers. Moreover, the expression of Rs_MEP1 in the transgenic lines was analyzed by qRT-PCR using gene-specific primers and the Arabidopsis actin gene as an endogenous control. The seeds of the positive transgenic lines were propagated to the T2 generation for further analysis.

dsRNA-mediated silencing of *Rs_MEP1*

The 356-bp region of *Rs_MEP1* and the 385-bp region of *Rs_GT34* that were used for HIGS were selected for dsRNA synthesis. The forward and reverse primers were designed to include a flanking region of the T7 RNA polymerase promoter. Partial gene fragments were amplified from the genomic DNA of *R. solani*. Purified gene fragments (1 µg) were used for in vitro transcription to produce dsRNA, using the MEGAscript T7 transcription kit (Thermo Scientific), according to the manufacturer's protocol. dsRNA (50 µg)- treated *R. solani* sclerotia were inoculated into plants (Ghosh et al. 2021). Infected plant samples were collected at 3 dpi. The expression was quantified by qRT-PCR using gene-specific primers. The buffer-treated and *Rs_GT34*-silenced *R. solani* (negative) were used as controls. The experiment was repeated thrice with at least three independent biological replicates.

Computational analysis

The presence of signal peptide (SP) in Rs-MEP1 was analyzed by *SignalP* searches (Almagro et al. 2019), whereas its subcellular localization was predicted by *EffectorP* (https://effectorp.csiro.au) (Sperschneider and Dodds 2022). Rs_MEP1 homologs in other fungal strains were identified by NCBI BLAST search. The conserved domain was identified using NCBI CDD search (https://www.ncbi.nlm.nih.gov/Structure/cdd/wrpsb.cgi/). The amino acid sequences were aligned by Clustal Omega

(https://www.ebi.ac.uk/jdispatcher/msa/clustalo/). Three-dimensional structural modeling of Rs_MEP1 was conducted by I-TASSER server (Zhou et al. 2022) (http://zhanglab.ccmb.med.umich.edu/I-TASSER). The I-TASSER performs automated protein structure homology modeling of query proteins using available crystal structures of homologous proteins as templates. Structural analogs of the protein were identified using the TM-align program in I-TASSER. The top-ranked predicted models, based on template modeling scores and accuracy assessment, were selected.

Subcellular localization of Rs_MEP1 in *Nicotiana benthamiana*

Rs_MEP1 encoding sequence with and without signal peptide lacking a stop codon was amplified from *R. solani* cDNA using gene-specific primers and Phusion DNA Polymerase (Thermo Fisher Scientific, USA). The PCR products were cloned into the binary vector pCAMBIA1302-GFP, having fused GFP under the 35S promoter. The recombinant plasmid and empty vector were individually introduced into *A. tumefaciens* strain GV3101. The cultures of the recombinant *A. tumefaciens* strains were grown, pelleted, and re-suspended in induction buffer (10 mM MES, 10 mM $MgCl_2$, 200 µM acetosyringone). The agrobacterial strain harboring p35S:Rs_MEP1-GFP was mixed in a 1:1 ratio with the strain expressing mCherry-tagged apoplast marker (pCMU-APr) (Ivanov and Harrison 2014). The resuspended cells (0.5 OD) were infiltrated into the 3-week-old *N. benthamiana* leaves with a 1 mL syringe without a needle (Chandan et al. 2023b). After infiltration, plants were incubated under a 12 h light/12 h dark photoperiodic cycle at 28°C. The subcellular localization was visualized after 48 h of infiltration under Leica TCSSP5 scanning microscope (Leica Microsystems). GFP and RFP signals were observed at 488–510 nm and 532–588 nm, respectively. For plasmolysis, leaf sections were excised, incubated in 1 M NaCl until epidermal cells were visibly plasmolyzed, and the fluorescence signal was examined by confocal microscopy, as described above.

Yeast secretion trap assay

Rs_MEP1 gene with and without SP was cloned in the upstream of the 5’ end of a yeast invertase (*suc2*) gene (lacking its SP) in pYST vector (Rs_MEP1/pYST), wherein transgene expression is regulated by ADH1 promoter. Rs_MEP1/pYST and pYST (vector control) plasmids were transformed into the *suc2* yeast mutant with Yeastmaker™ yeast transformation system following the manufacturer’s protocol. Transformed yeast cells were cultured on SD–Leu at 28 °C and spotted as 10-fold serial dilutions onto SD–Leu plates containing glucose or sucrose. Plates were incubated for 2 days at 28 °C. (Singh et al. 2023). The recombinant yeast

colonies (expressing Rs_MEP1 with and without signal peptide) were used as the test colonies. Yeast cells transformed with the pYST vector were used as a negative control.

Yeast two-hybrid assay

Yeast two-hybrid (Y2H) assay was performed using Matchmaker Gold Yeast two-hybrid library screening system (Clontech, USA). *Rs_MEP1* was cloned into the pGADT7-AD prey vector, and target rice chitinase genes (Os_04g41680 and Os_04g28080) were cloned into the pGBKT7-BD vector. Both bait and prey recombinant plasmids were co-transformed into a Y2H Gold strain of yeast, following the manufacturer's instructions. Positive transformants were selected on synthetically defined media lacking leucine and tryptophan amino acids (SD-Leu-Trp; double dropout). The interaction was confirmed by growing positive transformed colonies at 30°C on quadruple dropout media lacking leucine, tryptophan, histidine, and adenine (SD-Leu-Trp-His-Ade). The yeast cells co-transformed with pGBKT7 and pGADT7 (empty vectors) were used as a negative control, while the yeast cells co-transformed with pGBKT7-P53 and pGADT7-T (SV40 large T-antigen) were used as a positive control (Yadav et al. 2021). The experiment was independently repeated three times.

Bimolecular fluorescence complementation (BiFC) assay

Rs_MEP1 was cloned into the 35S-pSPYNE-YFP vector as an N-terminal fusion protein. The rice chitinase gene (Os_04g41680) was cloned into the 35S-pSPYCE-YFP vector as a C-terminal fusion protein. The plasmids were introduced into *A. tumefaciens* GV3101, and the bacterial culture was co-infiltrated into 3-week-old *N. benthamiana* leaves, at 0.5 OD. After 3 days post-infiltration, the reconstitution of YFP fluorescence was analyzed under a 514 nm laser of an SP2 AOBS confocal laser scanning microscope (Leica Microsystems) as described in (Chandan et al. 2023a). The experiment was independently repeated at least three times.

Transient expression of Rs_MEP1

Rs_MEP1 was cloned into a binary vector (pCAMBIA1302), and transformed into *A. tumefaciens* GV3101. The bacterial culture (0.8-1.0 OD) was infiltrated into rice and *N. benthamiana* leaves using a needle-less syringe (Sahoo et al. 2026). The plants were incubated under controlled conditions, and the appearance of cell death/ necrotic symptoms was monitored. The *A. tumefaciens* cells harboring an empty vector (pCAMBIA1302) were used as a control. Upon H_2DCFDA staining, ROS accumulation in the leaves was visualized under a confocal microscope. The crude protein extract was prepared from infiltrated leaves, as

described in (Sahoo et al. 2026), and immunoblot analysis was performed by electroblotting the protein onto a polyvinylidene fluoride (PVDF) membrane. The membrane was probed with mouse polyclonal anti-His-antibody (1:1000 dilutions), as described in (Yadav et al. 2021).

Expression and purification of protein

Rs_MEP1 was cloned into pET28(a), a bacterial expression vector and mobilized into *E. coli* (BL21) cells. Upon 1 mM IPTG (Isopropyl β- d-1-thiogalactopyranoside) induction for 3 h at 37 ^{0}C, bacterial cells were harvested and sonicated in lysis buffer [10 mM phosphate buffer saline (PBS); pH 7.4, 1 mM lysozyme, and 1 mM Phenyl methane sulfonyl fluoride (PMSF)]. Subsequently, the proteins were purified from the soluble fractions using Ni 2+- NTA beads (pre-equilibrated with 10 mM PBS; pH 7.4), as described earlier (Swain et al. 2017; Yadav et al. 2021). Immunoblot analysis was conducted by electroblotting the protein onto a PVDF membrane and probing with mouse polyclonal anti-His-antibody (1:1000 dilutions).

Chitinase activity assays

The chitinase activity was measured using a fluorometric assay with 4-Methylumbelliferyl N-acetyl-b-D-glucosaminide (Sigma Aldrich) as substrate (Huang et al. 2005). The amount of 4-methylumbelliferone (4-MU) released was measured using a fluorescence spectrophotometer (F-4500, Hitachi) (excitation 360 nm and emission 450 nm). One unit (U) of chitinase activity was defined as the amount of enzyme required to release one µmol of 4-MU per minute at 37^{o}C. Fluorescence was recorded in an acidic environment at three different concentrations of Rs_MEP1 protein. To perform the chitinase assay, 20 µg of Rs_MEP1 was mixed with an equal amount of chitinase enzyme (provided with the kit) and incubated at 37 °C for 30 min. The chitinase enzyme incubated without Rs_MEP1 was used as a control. To test the effect of Rs_MEP1 on rice chitinase, *A. tumefaciens* GV3101 strains expressing *Rs_MEP1* and/or rice chitinase (Os_04g41680, cloned in pCAMBIA1302) were infiltrated into *N. benthamiana* leaves. The crude protein was extracted from the agroinfiltrated leaves, as described in (Sahoo et al 2026), and the effect of Rs_MEP1 on rice chitinase activity was assessed using the fluorometric assay kit, as described above.

Preparation of alcohol insoluble residues (AIR)

The cell wall residue was prepared from the dried, powdered stem of *A. thaliana* by treating it with 70% ethanol at 50 0 C to remove soluble sugars. The pellet was further incubated with a chloroform: methanol mixture at room temperature for 10 min, followed by washing with water

and acetone. The remaining pellet was dried in a vacuum dryer overnight, and this AIR was used for the cell wall-degrading enzyme inhibition assay, as described in (Dewangan et al. 2023).

Xylanase Inhibition Assay

The 5 mg AIR or acetylated xylan (Megazyme, P-ACXYL, Ireland) was incubated with a mixture of GH11 xylanase (1 µl/mg) (SRL, 13814, India) and purified MEP (10 µl/mg or 15 µl/mg) in 50 mM of sodium acetate buffer (pH 4.5) for 3 h and 6 h. The supernatant was collected after centrifugation and analyzed using the xylose kit (Megazyme, K-Xylose, Ireland). The xylose release was calculated based on a standard curve as described in (Chaudhari et al. 2024).

Cellic CTec2 inhibition assay

The AIR was incubated with a mixture of CTec2 enzyme blend (Sigma-Aldrich, SAE0020, USA) (1 µl/mg) and purified MEP (10 µl/mg or 15 µl/mg) at 55 ^{0}C in 0.1M acetate buffer (pH 4.8) for 3 h and 6 h. The supernatant was collected after centrifugation, and glucose release was measured using the GOD-POD reagent (Megazyme, K-Gluc, Ireland), as follows. The 6 µl of Supernatant was mixed with 200 µl of GOD-POD reagent, and the mixture was incubated at 45 ^{0}C for 20 min, and absorbance was monitored at 510 nm. The glucose release was calculated based on the standard curve as described in (Chaudhari et al. 2024).

Statistical analysis

GraphPad Prism 8.0 was used to estimate statistical significance using one-way ANOVA, and Brown-Forsythe test/ Sidak's multiple comparison test. Two-way ANOVA and Tukey's test or Student's t-test were used to analyze the significance of the data shown in Figure 5. Significant difference with *p*-value of <0.05 or <0.001 is indicated by a star.

Acknowledgments

A.P. acknowledges SRF fellowship from University Grants Commission, Govt of India. G.J. acknowledges SR-NBACD award (HRD-20/3/2024-HRD-DBT) and project grants (BT/PR58439/BSA/33/550/2025 and BT/PR44291/AGIII/103/1349/2021) from DBT, Govt of India, and CRG grant (CRG/2022/004092) from ANRF (SERB), Govt of India, for supporting research in his lab. The authors acknowledge K Vengadesan and Shivangi Tyagi, Regional Centre for Biotechnology, Faridabad, for fruitful discussion. The assistance of NIPGR confocal

facility and the central instrumentation facilities is acknowledged. The authors are also thankful to DBT-eLibrary Consortium (DeLCON) for providing access to e-resources.

Funding information

The work is partially supported by Swarna Jayanti Fellowship (SB/SJF/2020-21/01) and CRG grant (CRG/2022/004092) from Anusandhan National Research Foundation (ANRF), Govt of India, and a core research grant from BRIC-National Institute of Plant Genome Research (NIPGR), New Delhi.

Author contributions

GJ planned the work and supervised its progress. AP carried out pathology and molecular biology experiments in this study. DS independently repeated the microscopic analysis. VB performed, and PP supervised, xylanase and CTec2 inhibition assay experiments. RK and RY performed rice chitinase inhibition assay and western blot analysis. SG assisted in bioinformatics analysis and initial standardization of dsRNA-mediated gene silencing. GJ and AP contributed to manuscript writing, and all authors approved the manuscript.

Conflict of interest

No conflict of interest was declared.

Data Availability

All data supporting the study are available within the article and its supplemental material.

Supplementary Data

Supplementary Table S1: List of candidate pathogenicity genes analyzed in this study.

Supplementary Table S2: Rs_MEP1 homologs in *R. solani* strains belonging to different anastomosis groups.

Supplementary Table S3: List of rice chitinase genes and their features.

Supplementary Table S4: List of primers used in this study.

Supplementary Figure 1. Disease severity in *R. solani*-infected HIGS tomato lines for selected candidate pathogenicity determinants.

Supplementary Figure 2. Domain architecture of Rs_MEP1.

Supplementary Figure 3. *Rs_MEP1* is an important pathogenicity determinant of *R. solani*.

Supplementary Figure 4. Infection cushion formation and depth of host penetration are compromised in *Rs_MEP1* HIGS tomato plants.

Supplementary Figure 5. dsRNA-mediated silencing of *Rs_MEP1* significantly compromises the pathogenesis of *R. solani* in tomato.

Supplementary Figure 6. Characterization of *Rs_MEP1* RNAi lines in *Arabidopsis.*

References

Almagro Armenteros, J.J., Tsirigos, K.D., Sønderby, C.K., Petersen, T.N., Winther, O., Brunak, S., von Heijne, G., and Nielsen, H. 2019. SignalP 5.0 improves signal peptide predictions using deep neural networks. Nat. Biotechnol. 37: 420-423

Ayliffe, M., Periyannan, S. K., Feechan, A., Dry, I., Schumann, U., Wang, M.-B., Pryor, A., and Lagudah, E. 2013. A Simple Method for Comparing Fungal Biomass in Infected Plant Tissues. Mol. Plant-Microbe Interact. 26:658–667

Chandan, R. K., Kumar, R., Kabyashree, K., Yadav, S. K., Roy, M., Swain, D. M., and Jha, G. 2023a. A prophage tail-like protein facilitates the endophytic growth of Burkholderia gladioli and mounting immunity in tomato. New Phytol. 240:1202–1218

Chandan, R. K., Kumar, R., Swain, D. M., Ghosh, S., Bhagat, P. K., Patel, S., Bagler, G., Sinha, A. K., and Jha, G. 2023b. RAV1 family members function as transcriptional regulators and play a positive role in plant disease resistance. Plant J. 114:39–54

Chaudhari, A. A., Sharma, A. M., Rastogi, L., Dewangan, B. P., Sharma, R., Singh, D., Sah, R. K., Das, S., Bhattacharjee, S., Mellerowicz, E. J., and Pawar, P. A. M. 2024. Modifying lignin composition and xylan O-acetylation induces changes in cell wall composition, extractability, and digestibility. Biotechnol. Biofuels Bioprod. 17:73

Clough, S. J., and Bent, A. F. 1998. Floral dip: a simplified method for Agrobacterium -mediated transformation of Arabidopsis thaliana. Plant J. 16:735–743

Das, J., Ghosh, S., Tyagi, K., Sahoo, D., and Jha, G. 2024. Methionine biosynthetic genes and methionine sulfoxide reductase A are required for Rhizoctonia solani AG1-IA to cause sheath blight disease in rice. Microb. Biotechnol. 17:e14441

de Jonge, R., Peter van Esse, H., Kombrink, A., Shinya, T., Desaki, Y., Bours, R., Van Der Krol, S., Shibuya, N., Joosten, M.H. and Thomma, B.P. 2010. Conserved fungal LysM effector Ecp6 prevents chitin-triggered immunity in plants. Science, 329: 953-955

Dewangan, B. P., Gupta, A., Sah, R. K., Das, S., Kumar, S., Bhattacharjee, S., and Pawar, P.

A. M. 2023. Xylobiose treatment triggers a defense-related response and alters cell wall composition. Plant Mol. Biol. 113:383-400

Feng, Z., Gao, P., Wang, G., Kang, H., Zhao, J., Xie, W., Chen, R., Ju, R., Wang, X., Wei, Z., Zhang, H., Zhang, J., Zhang, Y., Hu, K., Sun, Q., Zhu, Y., Xiong, Y., Liu, X., Chen, X., Chen, Z., Yang, C., Liu, J., Wang, G. L., Zhang, S. W., Yang, Z., and Zuo, S. 2025. Natural variation in SBRR1 shows high potential for sheath blight resistance breeding in rice. Nat. Genet. 57:2004-2016.

Fiorin, G.L., Sanchéz-Vallet, A., de Toledo Thomazella, D.P., do Prado, P.F.V., do Nascimento, L.C., de Oliveira Figueira, A.V., Thomma, B.P., Pereira, G.A.G. and Teixeira, P.J.P.L. 2018. Suppression of plant immunity by fungal chitinase-like effectors. Curr. Biol. 28: 3023-3030

Francis, A., Ghosh, S., Tyagi, K., Prakasam, V., Rani, M., Singh, N. P., Pradhan, A., Sundaram, R. M., Priyanka, C., Laha, G. S., Kannan, C., Prasad, M. S., Chattopadhyay, D., and Jha, G. 2023. Evolution of pathogenicity-associated genes in Rhizoctonia solani AG1-IA by genome duplication and transposon-mediated gene function alterations. BMC Biol. 21:15

Gebremichael, D. E., Haile, Z. M., Negrini, F., Sabbadini, S., Capriotti, L., Mezzetti, B., and Baraldi, E. 2021. RNA Interference Strategies for Future Management of Plant Pathogenic Fungi: Prospects and Challenges. Plants. 10:650

Ghosh, S., Gupta, S. K., and Jha, G. 2014. Identification and functional analysis of AG1-IA specific genes of Rhizoctonia solani. Curr. Genet. 60:327–341

Ghosh, S., Kant, R., Pradhan, A., and Jha, G. 2021. RS_CRZ1 , a C2H2-Type Transcription Factor Is Required for Pathogenesis of Rhizoctonia solani AG1-IA in Tomato. Mol. Plant-Microbe Interact. 34:26–38

Ghosh, S., Kanwar, P., and Jha, G. 2017. Alterations in rice chloroplast integrity, photosynthesis and metabolome associated with pathogenesis of Rhizoctonia solani. Sci. Rep. 7:41610

Ghosh, S., Kanwar, P., and Jha, G. 2018. Identification of candidate pathogenicity determinants of Rhizoctonia solani AG1-IA, which causes sheath blight disease in rice. Curr. Genet. 64:729–740

Ghosh, S., Mirza, N., Kanwar, P., Tyagi, K., and Jha, G. 2019. Genome analysis provides insight about pathogenesis of Indian strains of Rhizoctonia solani in rice. Funct. Integr. Genomics. 19:799–810

Gong, B.-Q., Wang, F.-Z., and Li, J.-F. 2020. Hide-and-Seek: Chitin-Triggered Plant Immunity and Fungal Counterstrategies. Trends Plant Sci. 25:805–816

Hane, J. K., Anderson, J. P., Williams, A. H., Sperschneider, J., and Singh, K. B. 2014. Genome Sequencing and Comparative Genomics of the Broad Host-Range Pathogen Rhizoctonia solani AG8 P.M. Richardson, ed. PLoS Genet. 10:e1004281

Huang, C.-J., Wang, T.-K., Chung, S.-C., and Chen, C.-Y. 2005. Identification of an Antifungal Chitinase from a Potential Biocontrol Agent, Bacillus cereus 28-9. BMB Rep. 38:82–88

Ivanov, S., and Harrison, M. J. 2014. A set of fluorescent protein-based markers expressed from constitutive and arbuscular mycorrhiza-inducible promoters to label organelles, membranes and cytoskeletal elements in Medicago truncatula. Plant J. 80:1151–1163.

Jashni, M.K., Dols, I.H., Iida, Y., Boeren, S., Beenen, H.G., Mehrabi, R., Collemare, J. and de Wit, P.J. 2015. Synergistic action of a metalloprotease and a serine protease from Fusarium oxysporum f. sp. lycopersici cleaves chitin-binding tomato chitinases, reduces their antifungal activity, and enhances fungal virulence. Mol. Plant-Microbe Interact. 28: 996-1008

Jia, Y., Liu, G., Park, D.-S., and Yang, Y. 2013. Inoculation and Scoring Methods for Rice Sheath Blight Disease. Pages 257–268

Kant, R., Tyagi, K., Ghosh, S., and Jha, G. 2019. Host Alternative NADH:Ubiquinone Oxidoreductase Serves as a Susceptibility Factor to Promote Pathogenesis of Rhizoctonia solani in Plants. Phytopathol. 109:1741–1750

Kuběnová, L., Haberland, J., Dvořák, P., Šamaj, J., and Ovečka, M. 2023. Spatiotemporal distribution of reactive oxygen species production, delivery, and use in Arabidopsis root hairs. Plant Physiol. 193:2337-2360

Lee, D.-Y., Jeon, J., Kim, K.-T., Cheong, K., Song, H., Choi, G., Ko, J., Opiyo, S. O., Correll, J. C., Zuo, S., Madhav, S., Wang, G.-L., and Lee, Y.-H. 2021. Comparative genome analyses of four rice-infecting Rhizoctonia solani isolates reveal extensive enrichment of homogalacturonan modification genes. BMC Genom. 22:242

Lee, S.-J., Kim, B.-D., and Rose, J. K. C. 2006. Identification of eukaryotic secreted and cell surface proteins using the yeast secretion trap screen. Nat. Protoc. 1:2439–2447

Liu, S., Liu, J., Wang, W., Yan, Y., Wang, T., Wu, J., Liu, X., Wu, J., and Zeng, Y. 2024. Comparative Field Evaluation and Transcriptome Analysis Reveals that Chromosome Doubling Enhances Sheath Blight Resistance in Rice. Rice. 17:42

Livak, K. J., and Schmittgen, T. D. 2001. Analysis of Relative Gene Expression Data Using Real-Time Quantitative PCR and the 2−ΔΔCT Method. Methods. 25:402–408

Lück, S., Kreszies, T., Strickert, M., Schweizer, P., Kuhlmann, M., and Douchkov, D. 2019. siRNA-Finder (si-Fi) Software for RNAi-Target Design and Off-Target Prediction. Front.

Plant Sci. 10:1023

Martínez-Cruz, J., Romero, D., Hierrezuelo, J., Thon, M., de Vicente, A., and Pérez-García, A. 2021. Effectors with chitinase activity (EWCAs), a family of conserved, secreted fungal chitinases that suppress chitin-triggered immunity. Plant Cell. 33:1319–1340

Molla, K. A., Karmakar, S., Molla, J., Bajaj, P., Varshney, R. K., Datta, S. K., and Datta, K. 2020. Understanding sheath blight resistance in rice: the road behind and the road ahead. Plant Biotechnol. J. 18:895–915

Morimoto, K., Krahn, D., Kaschani, F., Hopkinson-Woolley, D., Gee, A., Buscaill, P., Mohammed, S., Sieber, S.A., Cravatt, B.F., Schofield, C.J., and van der Hoorn, R.A. 2022. Broad-range metalloprotease profiling in plants uncovers immunity provided by defence-related metalloenzyme. New Phytol. 235:1287-1301

Naumann, T.A., Wicklow, D.T. and Price, N.P. 2011. Identification of a chitinase-modifying protein from Fusarium verticillioides: truncation of a host resistance protein by a fungalysin metalloprotease. J. Biol. Chem. 286: 35358-35366

Nielsen, H., Teufel, F., Brunak, S., and von Heijne, G. 2024. SignalP: the evolution of a web server. In Protein bioinformatics. New York, NY: Springer US. 331-367

Niu, X., Yang, G., Lin, H., Liu, Y., Li, P., and Zheng, A. 2021. A Novel, Small Cysteine-Rich Effector, RsSCR10 in Rhizoctonia solani Is Sufficient to Trigger Plant Cell Death. Front. Microbiol. 12:684923

Ökmen, B., Kemmerich, B., Hilbig, D., Wemhöner, R., Aschenbroich, J., Perrar, A., Huesgen, P. F., Schipper, K., and Doehlemann, G. 2018. Dual function of a secreted fungalysin metalloprotease in Ustilago maydis. New Phytol. 220:249–261

Pan, L., Lu, L., Liu, Y., Wen, S., and Zhang, Z. 2020. The M43 domain-containing metalloprotease RcMEP1 in Rhizoctonia cerealis is a pathogenicity factor during the fungus infection to wheat. J. Integr. Agric. 19: 2044-2055

Pradhan, A., Ghosh, S., Sahoo, D., and Jha, G. 2021. Fungal effectors, the double edge sword of phytopathogens. Curr. Genet. 67:27–40

Rani, M., and Jha, G. 2021. Host Gamma-Aminobutyric Acid Metabolic Pathway Is Involved in Resistance Against Rhizoctonia solani. Phytopathol. 111:1207–1218

Rocafort, M., Fudal, I., and Mesarich, C.H. 2020. Apoplastic effector proteins of plant-associated fungi and oomycetes. Curr. Opin. Plant Biol. 56: 9-19.

Sahoo, D., Chandan, R.K., Goel, N., and Jha, G. 2026. OsNUOR enhances disease susceptibility by interfering with reactive oxygen species homeostasis and ferroptosis-like

cell death. The Plant Cell, 38: koag112

Sanz-Martín, J. M., Pacheco-Arjona, J. R., Bello-Rico, V., Vargas, W. A., Monod, M., Díaz-Mínguez, J. M., Thon, M. R., and Sukno, S. A. 2016. A highly conserved metalloprotease effector enhances virulence in the maize anthracnose fungus Colletotrichum graminicola. Mol. Plant Pathol. 17:1048–1062

Senapati, M., Tiwari, A., Sharma, N., Chandra, P., Bashyal, B. M., Ellur, R. K., Bhowmick, P. K., Bollinedi, H., Vinod, K. K., Singh, A. K., and Krishnan, S. G. 2022. Rhizoctonia solani Kühn Pathophysiology: Status and Prospects of Sheath Blight Disease Management in Rice. Front. Plant Sci. 13:881116

Singh, P., Mazumdar, P., Harikrishna, J. A., and Babu, S. 2019. Sheath blight of rice: a review and identification of priorities for future research. Planta. 250:1387–1407

Singh, S. K., Shree, A., Verma, S., Singh, K., Kumar, K., Srivastava, V., Singh, R., Saxena, S., Singh, A. P., Pandey, A., and Verma, P. K. 2023. The nuclear effector ArPEC25 from the necrotrophic fungus Ascochyta rabiei targets the chickpea transcription factor CaβLIM1a and negatively modulates lignin biosynthesis, increasing host susceptibility. Plant Cell. 35:1134–1159

Sperschneider, J., and Dodds, P.N. 2022. EffectorP 3.0: prediction of apoplastic and cytoplasmic effectors in fungi and oomycetes. Molecular plant-microbe interactions, 35:146-156.

Swain, D. M., Yadav, S. K., Tyagi, I., Kumar, R., Kumar, R., Ghosh, S., Das, J., and Jha, G. 2017. A prophage tail-like protein is deployed by Burkholderia bacteria to feed on fungi. Nat. Commun. 8:404

van den Burg, H.A., Harrison, S.J., Joosten, M.H., Vervoort, J., and de Wit, P.J. 2006. Cladosporium fulvum Avr4 protects fungal cell walls against hydrolysis by plant chitinases accumulating during infection. Mol. Plant-Microbe Interact. 19: 1420-1430

Tariqjaveed, M., Mateen, A., Wang, S., Qiu, S., Zheng, X., Zhang, J., Bhadauria, V., and Sun, W. 2021. Versatile effectors of phytopathogenic fungi target host immunity. J. Integr. Plant Biol. 63:1856–1873

Wang, A., Shu, X., Jing, X., Jiao, C., Chen, L., Zhang, J., Ma, L., Jiang, Y., Yamamoto, N., Li, S., Deng, Q., Wang, S., Zhu, J., Liang, Y., Zou, T., Liu, H., Wang, L., Huang, Y., Li, P., and Zheng, A. 2021. Identification of rice (Oryza sativa L.) genes involved in sheath blight resistance via a genome-wide association study. Plant Biotechnol. J. 19:1553–1566

Wibberg, D., Andersson, L., Tzelepis, G., Rupp, O., Blom, J., Jelonek, L., Pühler, A., Fogelqvist, J., Varrelmann, M., Schlüter, A., and Dixelius, C. 2016. Genome analysis of the sugar beet pathogen Rhizoctonia solani AG2-2IIIB revealed high numbers in secreted

proteins and cell wall degrading enzymes. BMC Genom. 17:245

Willocquet, L., Lore, J. S., Srinivasachary, S., and Savary, S. 2011. Quantification of the Components of Resistance to Rice Sheath Blight Using a Detached Tiller Test Under Controlled Conditions. Plant Dis. 95:1507–1515

Yadav, S. K., Magotra, A., Ghosh, S., Krishnan, A., Pradhan, A., Kumar, R., Das, J., Sharma, M., and Jha, G. 2021. Immunity proteins of dual nuclease T6SS effectors function as transcriptional repressors. EMBO Rep. 22:e51857

Zhang, D., Lin, R., Yamamoto, N., Wang, Z., Lin, H., Okada, K., Liu, Y., Xiang, X., Zheng, T., Zheng, H., Yi, X., Noutoshi, Y., and Zheng, A. 2024. Mitochondrial-targeting effector RsIA_CtaG/Cox11 in Rhizoctonia solani AG-1 IA has two functions: plant immunity suppression and cell death induction mediated by a rice cytochrome c oxidase subunit. Mol. Plant Pathol. 25:e13397

Zheng, A., Lin, R., Zhang, D., Qin, P., Xu, L., Ai, P., Ding, L., Wang, Y., Chen, Y., Liu, Y., Sun, Z., Feng, H., Liang, X., Fu, R., Tang, C., Li, Q., Zhang, J., Xie, Z., Deng, Q., Li, S., Wang, S., Zhu, J., Wang, L., Liu, H., and Li, P. 2013a. The evolution and pathogenic mechanisms of the rice sheath blight pathogen. Nat. Commun. 4:1424

Zheng, A., Lin, R., Zhang, D., Qin, P., Xu, L., Ai, P., Ding, L., Wang, Y., Chen, Y., Liu, Y., Sun, Z., Feng, H., Liang, X., Fu, R., Tang, C., Li, Q., Zhang, J., Xie, Z., Deng, Q., Li, S., Wang, S., Zhu, J., Wang, L., Liu, H., and Li, P. 2013b. The evolution and pathogenic mechanisms of the rice sheath blight pathogen. Nat. Commun. 4:1424

Zhou, X., Zheng, W., Li, Y., Pearce, R., Zhang, C., Bell, E. W., Zhang, G., and Zhang, Y. 2022. I-TASSER-MTD: a deep-learning-based platform for multi-domain protein structure and function prediction. Nat. Protoc. 17:2326–2353

Zrenner, R., Genzel, F., Verwaaijen, B., Wibberg, D., and Grosch, R. 2020. Necrotrophic lifestyle of Rhizoctonia solani AG3-PT during interaction with its host plant potato as revealed by transcriptome analysis. Sci. Rep. 10:12574

Figure Legends

Figure 1. Rs_MEP1 is a potential apoplastic effector protein of *R. solani*. **A.** Schematic representation of different domains present in the Rs_MEP1 protein. **B.** Vector map used to construct Rs_MEP1: SUC2ΔSP fusion protein for yeast signal sequence trap (YSST) assay. **C.** Yeast secretion trap assay, showing the growth of suc2 mutant yeast expressing Rs_MEP1/ Rs_MEP1ΔSP (signal peptide deleted variant)/ pYST vector (vector control) on synthetic

dropout (SD-Leu) media with sucrose/ glucose as a sole carbon source. The growth of yeast cells on SD-Leu + sucrose suggests the functional signal peptide. **D.** Subcellular localization of Rs_MEP1 and Rs_MEP1ΔSP in *N. benthamiana* leaves, with and without plasmolysis. GFP-tagged Rs_MEP1 and mCherry-tagged apoplast marker (pCMU-APr) were found to be co-localized. The GFP was visualized under GFP (green fluorescent protein) filter, while mCherry was visualized under RFP (red fluorescent protein) filter of the confocal microscope. The white arrows indicate an enlarged apoplast visible after plasmolysis. Similar results were obtained in at least three independent biological replicates, and representative images are shown. Scale bar: 20 μm.

Figure 2: The dsRNA-mediated silencing of *Rs_MEP1* significantly compromises the pathogenesis of *R. solani* in rice. **A**. qRT-PCR-based expression analysis of *R. solani* genes (*Rs_MEP1* and *Rs_GT34*) in dsRNA-treated and buffer-treated *R. solani* (WT) sclerotia. *R. solani 18S rRNA* gene was used as an endogenous control for normalizing gene expression. *Rs_GT34* is used as a negative control. **B**. Upper panel, disease symptoms in rice sheaths, infected with *Rs_MEP1*-silenced, *Rs_GT34*-silenced, and WT sclerotia, at 3 dpi. Lower panel, DAB staining of the infected sheaths, showing ROS accumulation. **C**. Relative vertical sheath colonization (RVSC) index showing disease severity, and **D**. Pathogen load, estimated as a relative abundance of *R. solani 18S rRNA* in the infected rice, at 3 dpi. The rice *18S rRNA* gene was used as an endogenous control for normalizing gene expression during qRT-PCR. The graph shows mean values ± standard error of three biological replicates. **E**, **F**, and **G**. Confocal microscopic analysis of WGA-FITC-stained rice sheaths showing significantly reduced colonization of *Rs_MEP1*-silenced *R. solani*. **E.** Confocal images showing fungal invasion in the sheaths. Red arrow indicates invasive hyphae. **F.** Topological overview showing depth of host penetration. Z-axis indicated as a coloured index bar, represents penetration depth. **G.** The bar graph showing the depth of host penetration. The data show the mean ± standard error across three independent biological replicates, with at least three infected leaf samples analyzed in each replicate. '**' indicates a significant difference at $p \leq 0.001$. Scale bar: 100 μm.

Figure 3. Rs_MEP1 induces cell death and enhances ROS accumulation in plants. Agrobacterium-mediated transient expression of Rs_MEP1 induces cell death in **A**. rice and **B.** *N. benthamiana* leaves, at 5 dpi. **C.** H_2DCFDA staining showing that expression of Rs_MEP1 enhanced ROS accumulation in the infiltrated regions. **D.** Immunoblot using anti-His antibody, reflecting accumulation of Rs_MEP1 (30 kDa) in rice and *N. benthamiana* samples. The

infiltration of the Agrobacterium strain transformed with an empty vector (pCAMBIA1302) was used as a vector control. Similar results were obtained in at least three independent biological replicates, and representative images are shown. Scale: 100 μm.

Figure 4. Rs_MEP1 physically interacts with rice chitinases. **A.** qRT-PCR-based expression profile of rice chitinase genes, upon *R. solani* infection, at different time points. The fold change in gene expression was estimated relative to 0 dpi, using rice 18S rRNA for normalization. **B.** Yeast two-hybrid assay reflecting positive interaction of Rs_MEP1 with one of the chitinases (Os_04g41680). The interaction between p53 and the SV40 large T-antigen (RecT) was used as a positive control. The pGBKT7 and pGADT7 (empty vectors) were used as a negative control. **C.** Bimolecular fluorescence complementation (BiFC) analysis showing *in-planta* interaction of Rs_MEP1 with Os_04g41680 in *N. benthamina* leaves. The Rs_MEP1 and Os_04g41680 were co-expressed as an N-terminal and a C-terminal YFP fusion protein, respectively. The mCherry-tagged pCMU-APr was used as an apoplast marker. The reconstitution of yellow fluorescence, colocalizing with mCherry-tagged apoplast marker (pCMU-APr) suggests physical interaction in the apoplast (indicated by white arrows). The YFP was visualized under YFP (yellow fluorescent protein) filter, while mCherry was visualized under RFP (red fluorescent protein) filter of the confocal microscope. . The pSPYNE and pSPYCE (empty vectors) were used as a negative control. Scale bars = 20 μm. Similar results were obtained in at least three independent biological replicates, and representative images are shown. **D.** Bar graph showing effect of Rs_MEP1 on chitinase activity, measured by estimating the released 4-Methylumbelliferone from the substrate using a microplate reader (excitation wavelength: 360 nm, and emission wavelength: 450 nm). **E.** Bar graph showing Rs_MEP1 inhibits rice chitinase (Os_04g41680) activity, when transiently expressed in *N. benthamiana* leaves, at 24 and 48 hours after agrobacterial infiltration. The data show the mean values ± standard error of three independent biological replicates. '*' indicates a significant difference at $p \leq 0.05$. Different letters represent a significant difference at $p < 0.05$. Data represent the mean of three independent biological replicates, each with three technical replicates.

Figure 5. Inhibition assay of xylanase and CTec2, a cocktail of cell wall-degrading enzymes, using xylan and complex cell wall as substrates. **A** and **B** show xylose release after digestion with xylanase (Xyl) and Rs_MEP1 (MEP) at different proportions, using pure xylan as the substrate. **C** and **D** represent the digestion of alcohol insoluble residue (complex cell wall)

using Xyl and CTec2, a cocktail of cell wall-degrading enzymes (Cel), respectively. Xylose and glucose were quantified using the Megazyme K-Xylose assay and the Megazyme K-Gluc assay kit, respectively. The bar graph represents mean ± SD. n = 2-4 replicates. Statistics are performed using 2-way ANOVA with multiple comparisons, and asterisks indicate significant differences at ** $p \leq 0.05$ using the Tukey test or student's t-test. We have highlighted only significant differences relative to the xylanase-treated samples. ns – non-significant.

Figure 6. Model summarizing the role of *Rs_MEP1* in promoting *R. solani* infection in plants. Upon pathogen perception, plants upregulate chitinases to degrade fungal chitin and induce chitin-triggered immunity, which prevents fungal infections. We observed several chitinase genes to be induced upon *R. solani* infection in rice. Our data emphasize that to counterbalance host response, *R. solani* deploys Rs_MEP1 to inactivate chitinases. This protects the integrity of the fungal cell wall and prevents the activation of chitin-triggered immunity, overall rendering plants susceptible to infection.

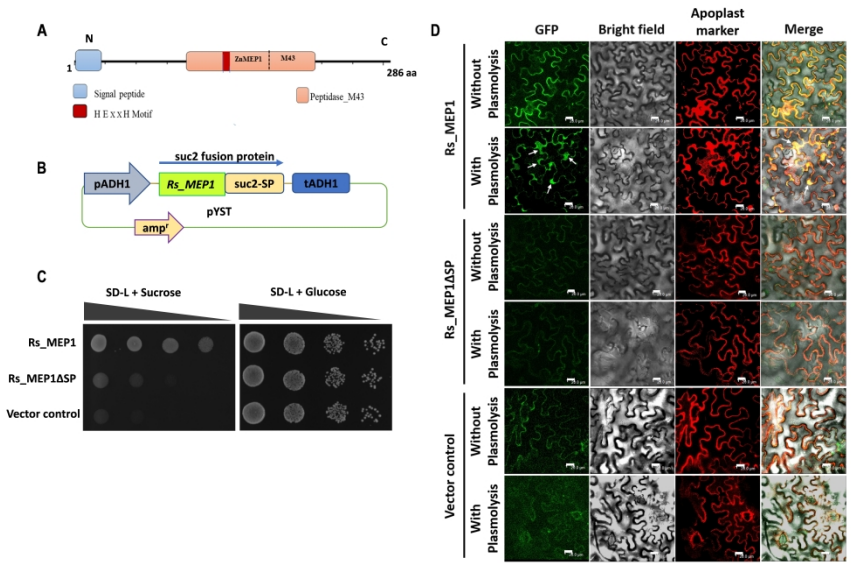

Figure 1. Rs_MEP1 is a potential apoplastic effector protein of R. solani. A. Schematic representation of different domains present in the Rs_MEP1 protein. B. Vector map used to construct Rs_MEP1: SUC2ΔSP fusion protein for yeast signal sequence trap (YSST) assay. C. Yeast secretion trap assay, showing the growth of suc2 mutant yeast expressing Rs_MEP1/ Rs_MEP1ΔSP (signal peptide deleted variant)/ pYST vector (vector control) on synthetic dropout (SD-Leu) media with sucrose/ glucose as a sole carbon source. The growth of yeast cells on SD-Leu + sucrose suggests the functional signal peptide. D. Subcellular localization of Rs_MEP1 and Rs_MEP1ΔSP in N. benthamiana leaves, with and without plasmolysis. GFP-tagged Rs_MEP1 and mCherry-tagged apoplast marker (pCMU-APr) were found to be co-localized. The GFP was visualized under GFP (green fluorescent protein) filter, while mCherry was visualized under RFP (red fluorescent protein) filter of the confocal microscope. The white arrows indicate an enlarged apoplast visible after plasmolysis. Similar results were obtained in at least three independent biological replicates, and representative images are shown. Scale bar: 20 µm.

1693x952mm (120 x 120 DPI)

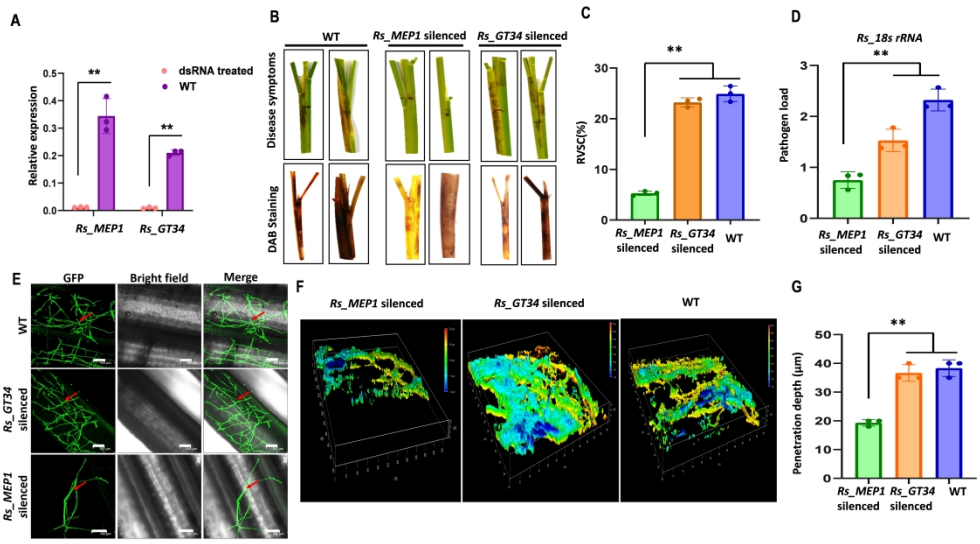

Figure 2: The dsRNA-mediated silencing of Rs_MEP1 significantly compromises the pathogenesis of R. solani in rice. A. qRT-PCR-based expression analysis of R. solani genes (Rs_MEP1 and Rs_GT34) in dsRNA-treated and buffer-treated R. solani (WT) sclerotia. R. solani 18S rRNA gene was used as an endogenous control for normalizing gene expression. Rs_GT34 is used as a negative control. B. Upper panel, disease symptoms in rice sheaths, infected with Rs_MEP1-silenced, Rs_GT34-silenced, and WT sclerotia, at 3 dpi. Lower panel, DAB staining of the infected sheaths, showing ROS accumulation. C. Relative vertical sheath colonization (RVSC) index showing disease severity, and D. Pathogen load, estimated as a relative abundance of R. solani 18S rRNA in the infected rice, at 3 dpi. The rice 18S rRNA gene was used as an endogenous control for normalizing gene expression during qRT-PCR. The graph shows mean values ± standard error of three biological replicates. E, F, and G. Confocal microscopic analysis of WGA-FITC-stained rice sheaths showing significantly reduced colonization of Rs_MEP1-silenced R. solani. E. Confocal images showing fungal invasion in the sheaths. Red arrow indicates invasive hyphae. F. Topological overview showing depth of host penetration. Z-axis indicated as a coloured index bar, represents penetration depth. G. The bar graph showing the depth of host penetration. The data show the mean ± standard error across three independent biological replicates, with at least three infected leaf samples analyzed in each replicate. '**' indicates a significant difference at $p \leq 0.001$. Scale bar: 100 µm.

1693x952mm (120 x 120 DPI)

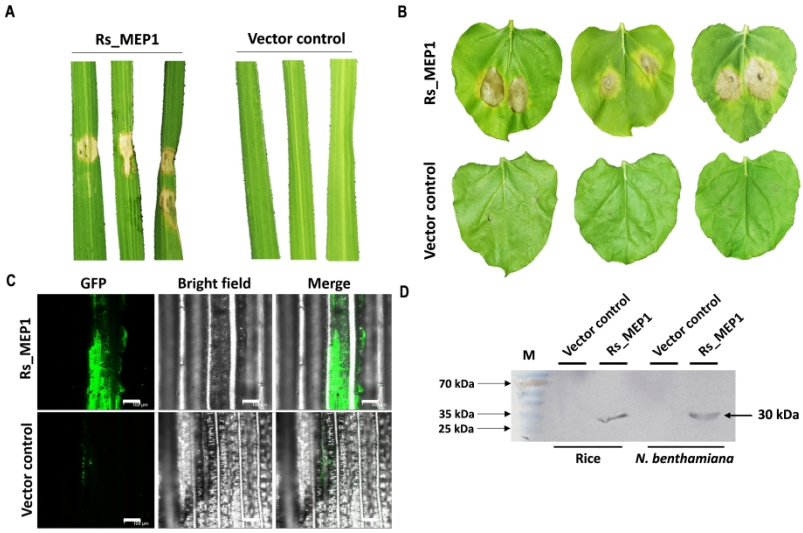

Figure 3. Rs_MEP1 induces cell death and enhances ROS accumulation in plants. Agrobacterium-mediated transient expression of Rs_MEP1 induces cell death in A. rice and B. N. benthamiana leaves, at 5 dpi. C. H2DCFDA staining showing that expression of Rs_MEP1 enhanced ROS accumulation in the infiltrated regions. D. Immunoblot using anti-His antibody, reflecting accumulation of Rs_MEP1 (30 kDa) in rice and N. benthamiana samples. The infiltration of the Agrobacterium strain transformed with an empty vector (pCAMBIA1302) was used as a vector control. Similar results were obtained in at least three independent biological replicates, and representative images are shown. Scale: 100 μm.

1693x952mm (120 x 120 DPI)

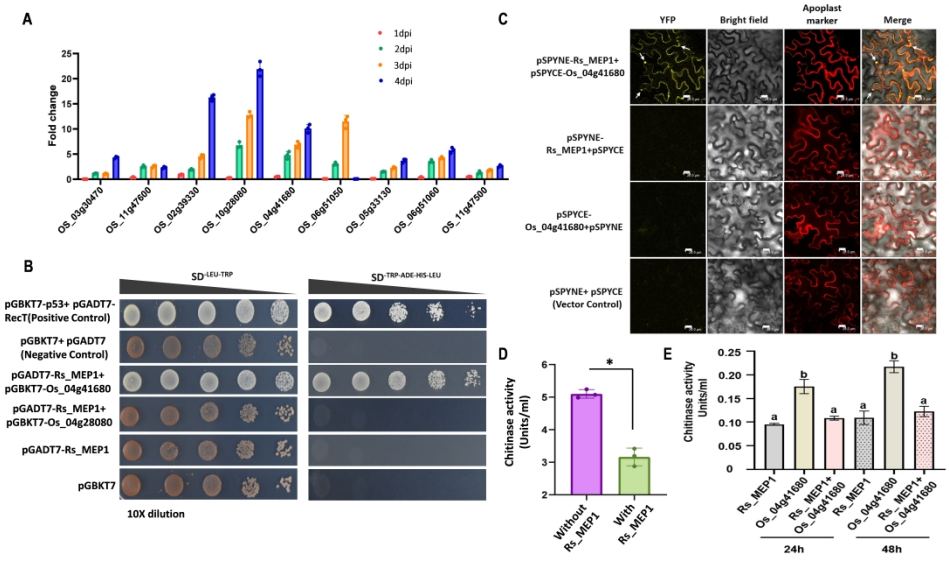

Figure 4. Rs_MEP1 physically interacts with rice chitinases. A. qRT-PCR-based expression profile of rice chitinase genes, upon R. solani infection, at different time points. The fold change in gene expression was estimated relative to 0 dpi, using rice 18S rRNA for normalization. B. Yeast two-hybrid assay reflecting positive interaction of Rs_MEP1 with one of the chitinases (Os_04g41680). The interaction between p53 and the SV40 large T-antigen (RecT) was used as a positive control. The pGBKT7 and pGADT7 (empty vectors) were used as a negative control. C. Bimolecular fluorescence complementation (BiFC) analysis showing in-planta interaction of Rs_MEP1 with Os_04g41680 in N. benthamina leaves. The Rs_MEP1 and Os_04g41680 were co-expressed as an N-terminal and a C-terminal YFP fusion protein, respectively. The mCherry-tagged pCMU-APr was used as an apoplast marker. The reconstitution of yellow fluorescence, colocalizing with mCherry-tagged apoplast marker (pCMU-APr) suggests physical interaction in the apoplast (indicated by white arrows). The YFP was visualized under YFP (yellow fluorescent protein) filter, while mCherry was visualized under RFP (red fluorescent protein) filter of the confocal microscope. . The pSPYNE and pSPYCE (empty vectors) were used as a negative control. Scale bars = 20 µm. Similar results were obtained in at least three independent biological replicates, and representative images are shown. D. Bar graph showing effect of Rs_MEP1 on chitinase activity, measured by estimating the released 4-Methylumbelliferone from the substrate using a microplate reader (excitation wavelength: 360 nm, and emission wavelength: 450 nm). E. Bar graph showing Rs_MEP1 inhibits rice chitinase (Os_04g41680) activity, when transiently expressed in N. benthamiana leaves, at 24 and 48 hours after agrobacterial infiltration. The data show the mean values ± standard error of three independent biological replicates. '*' indicates a significant difference at $p \leq 0.05$. Different letters represent a significant difference at $p < 0.05$. Data represent the mean of three independent biological replicates, each with three technical replicates.

1693x952mm (120 x 120 DPI)

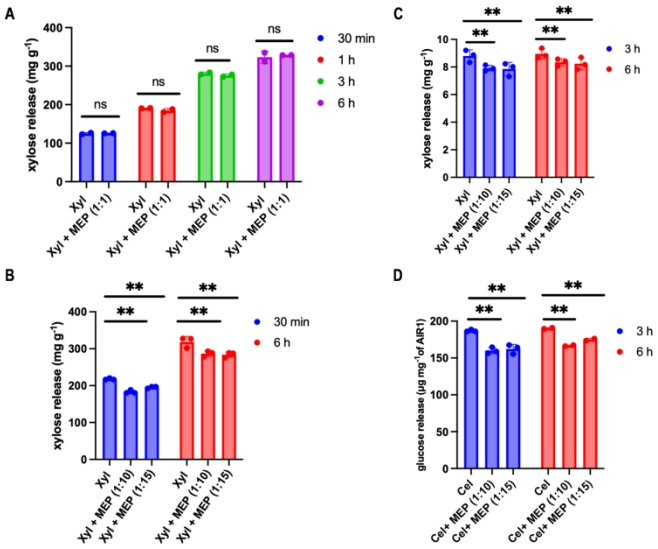

Figure 5. Inhibition assay of xylanase and CTec2, a cocktail of cell wall-degrading enzymes, using xylan and complex cell wall as substrates. A and B show xylose release after digestion with xylanase (Xyl) and Rs_MEP1 (MEP) at different proportions, using pure xylan as the substrate. C and D represent the digestion of alcohol insoluble residue (complex cell wall) using Xyl and CTec2, a cocktail of cell wall-degrading enzymes (Cel), respectively. Xylose and glucose were quantified using the Megazyme K-Xylose assay and the Megazyme K-Gluc assay kit, respectively. The bar graph represents mean ± SD. n = 2-4 replicates. Statistics are performed using 2-way ANOVA with multiple comparisons, and asterisks indicate significant differences at ** $p \leq 0.05$ using the Tukey test or student's t-test. We have highlighted only significant differences relative to the xylanase-treated samples. ns – non-significant.

1693x952mm (120 x 120 DPI)

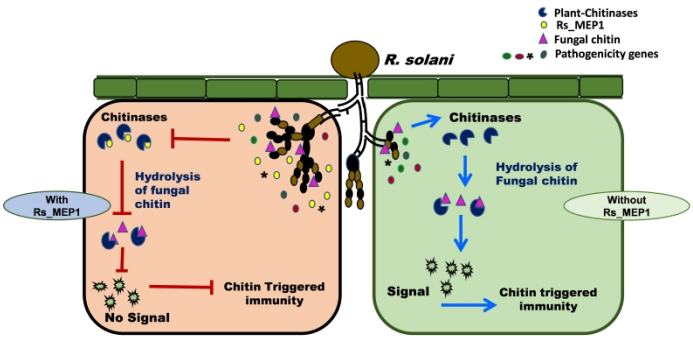

Figure 6. Model summarizing the role of Rs_MEP1 in promoting R. solani infection in plants. Upon pathogen perception, plants upregulate chitinases to degrade fungal chitin and induce chitin-triggered immunity, which prevents fungal infections. We observed several chitinase genes to be induced upon R. solani infection in rice. Our data emphasize that to counterbalance host response, R. solani deploys Rs_MEP1 to inactivate chitinases. This protects the integrity of the fungal cell wall and prevents the activation of chitin-triggered immunity, overall rendering plants susceptible to infection.

1693x952mm (120 x 120 DPI)

Supplementary Table S1: List of candidate pathogenicity genes analyzed in this study

S.N.	Gene Name[#]	Function	Upregulation pattern (Source- Ghosh et al. 2018)
1.	*Rs_AOX1* (alternate oxidase)	Alternative oxidative pathway	Both necrotrophic and establishment phase
2.	*Rs_GT34* (Glycosyl Transferase Family 34)	Cell wall-degrading enzyme	Necrotrophic phase
3.	*Rs_GzZC236* (*GATA* type zinc finger)	Transcription factor	Establishment phase
4.	*Rs_GAS1*(encoding β-1,3-glucanosyltransferase)	Appressorial penetration-associated proteins	Both phase
5.	*Rs_GST* (General substrate transporter)	Sugar transporters	Necrotrophic phase
6.	*Rs_ABC3*(ATP-binding cassette)	ABC Transporter	Establishment phase
7.	*Rs_PHO84* (phosphate transporter 84)	Phosphate transporter	Establishment phase
8.	*Rs_SPM1*	Protein degradation	Necrotrophic phase
9.	*Rs_MEP1* (Metalloprotease 1)	Protein degradation	Necrotrophic phase

#: These genes were selected from previously reported expression analysis (RNA-seq) of *R. solani* genes during infection in rice (Ghosh et al. 2018).

Supplementary Table S2: Rs_MEP1 homologs in *R. solani* strains belonging to different anastomosis groups

S.N.	Organism name	Present/Absent	Date of analysis
1.	*Rhizoctonia solani* AG-3 Rhs1AP	Present (EUC66575.1)	3/01/2024
2.	*R. solani* AG-1 IB	Present (CCO28218.1)	3/01/2024
3.	*R. solani* AG-1 IA	Present (ELU45660.1)	3/01/2024
4.	*R. solani* AG-8 WAC10335	Present (KDN40487.1)	3/01/2024
5.	*R. solani* AG-2	Absent	3/01/2024
6.	*R. solani* AG-4	Absent	3/01/2024
7.	*R. solani* AG-5	Absent	3/01/2024

Supplementary Table S3: List of rice chitinase genes and their features

S. N.	Locus I.D.	Length (aa)	Domains	Class	Fold change in expression #
1.	Os03g304750	326 aa	CBD, GH 19	Class I, Endochitinase	3.1
2.	Os11g47600	301 aa	GH 18	Chitinase III	3.3
3.	Os02g39330	271 aa	CBD, GH 19	Class IV, Endochitinase	3.7
4.	Os10g28080	286 aa	GH 18	Class III	4.8
5.	Os06g51060	349 aa	CBD, GH 19	Class I, Endochitinase	6.1
6.	Os04g41680	288 aa	CBD, GH 19	Class IV, Endochitinase	7.4
7.	Os06g51050	320 aa	CBD, GH 19	Class I, Endochitinase	6.5
8.	Os03g30470	326 aa	CBD, GH 19	Class I, Endochitinase	3.0
9.	Os05g33130	340 aa	CBD, GH 19	Class I, Endochitinase	7.2

#: The expression of the chitinase genes is taken from the previously reported *R. solani*-infected rice transcriptome data (Ghosh et al. 2017).

Supplementary Table S4: List of primers used in this study

Gene Name	Sequence
For HIGS-based constructs	
PDS	FP- 5'GAGCTCATGGGATAAGTGTTAAGGACTGGA 3'
	RP- 5'TCTAGAATCCACTGGAGCGGCAAAC 3'
TRV1-MP	FP- 5'CGGTAGGAGGAAGAGACCGA 3'
	RP- 5'AAGGACCATCGTACTTCGCC 3'
TRV2-Rs_GT34	FP- 5'GAATTCTGTATGGGCGTTGTGTGTGA 3'
	RP- 5'ACGCGTCCATGCTGCTAGTAGGGACG 3'
TRV2-Rs_MEP1	FP- 5'GAATTC TGTTCTCTGCGCTCTCTGTC 3'
	RP- 5'GGATCC AGAGTTGAACCAGTTCGCGT 3'
TRV2-Rs_ABC3	FP- 5'GGATCC GCCTGGGGATCGAGTTTCAA 3'
	RP- 5'ACGCGTAGGTCAGCAAAAGGGGTGAG 3'
TRV2- Rs_GzZC236	FP- 5'GAATTC GCCATTACGGACAATCGCAC 3'
	RP- 5'GGATCC AGCTCGCCCAAGGAATTTGA 3'
TRV2-Rs_ GAS1	FP- 5'GGATCC CTATACACAGACCGCGCCAT 3'
	RP- 5'ACGCGTTTCGTAACCTTTCGGCTGCT 3'
TRV2-Rs_ AOX1	FP- 5'GAATTC CAGCCACGCCGTATGACTAT 3'
	RP- 5'GGATCC TTTTCAAGTGCAGCGTTCGG 3'
TRV2-Rs_ SPM1	FP- 5'TCTAGACATCCTCCCTGCTCTTGGTG 3'
	RP- 5'ACGCGTTCAACTTCTCGGGGACAACG 3'
TRV2-Rs_ GST	FP- 5'GGATCC GTCAATGACTGCCACGGGTA 3'
	RP- 5'ACGCGTTCGCCGTCCTGAAAAGACTC 3'
TRV2-Rs_ PHO84	FP- 5'GAATTC GGGTTTCGGCTACGACAAGA 3'
	RP- 5'GGATCC TCGCGAAGAGACCAGTCAAC 3'
For localization study	
Pcam1302-Rs_MEP1	FP- 5'CCATGGATGTTGTTCTCTGCGCTCTCTGTCCTTG 3'
	RP- 5'ACTAGTGACGGTGATACCACGGTAAGTAGCGATTT 3'
Pcam1302-Rs_MEP1-SP	FP- 5'CCATGGATGTACTACAACCACACCATCTCCAGGAGCT 3'
	RP- 5'ACTAGTGACGGTGATACCACGGTAAGTAGCGATTT 3'
For Yeast two-hybrid study	
Os_04g41680 -PET28a	FP- 5'AAGCTTATGGCGAACTCACCGACGCCGAC 3'
	RP- 5'GAATTCACAGTAAAGGTTGCCACCCGGGTC 3'
RS_MEP1-PET28a	FP- 5'GCGGCCGCGACGGTGATACCACGGTAAGT 3'
	RP- 5'GCGGCCGCTTAGACGGTGATACCACGGTAAG 3'
PgktRs_MEP1	FP- 5'AATTCGAATTCATGTTGTTCTCTGCGCTCTCT 3'
	RP- 5'AATTCGTCGACGACGGTGATACCACGGTAAG 3'
pGADT7 Rs_MEP1	FP- 5'AATTCGAATTCATGTTGTTCTCTGCGCTCTCT 3'
	RP- 5'GAGCTCGACGGTGATACCACGGTAAG 3'
pGADT7Os_04g41680	FP- 5'GAATTCATGGCGAACTCACCGACGCC 3'
	RP- 5'GAGCTCACAGTAAAGGTTGCCACCCG 3'
pGADT7Os_03g30470	FP- 5'GAATTCATGAGAGCGCTCGCTGTGG 3'

	RP- 5’AATTCCTCGAGGGAGCCGAAGGGCCTCTGG 3’
pGADT7Os_11g47600	FP- 5’AATTCGAATTCATGGCGCGCCACCAGCTATGT 3’
	RP- 5’AATTCCTCGAGAACGAAGTCCTTGAGCGCCCT 3’
pGADT7Os_02g39330	FP- 5’AATTCGAATTCATGGCGCGAAGGCTCTCG 3’
	RP- 5’AATTCGAGCTCGCAGGTGAGGTTGCTGCCGG 3’
pGADT7Os_10g28080	FP- 5’AATTCGAATTCATGGTGAACGGCTACTTGT 3’
	RP- 5’AATTCCTCGAGGTGGTTGGCGACGATCTC 3’
pGADT7Os_06g51060	FP- 5’AATTCGAATTCATGCGCTCCCACCGCTTCTTA 3’
	RP- 5’AATTCCTCGAGGGAGTTGAAAGGCCTCTGGTTG 3’
pGADT7Os_06g51050	FP- 5’AATTCGAATTCATGAGAGCTCTCGCTCTCGC 3’
	RP- 5’AATTCCTCGAGGGAAGGCGGGTAGGGCCTCT 3’
pGADT7Os_05g33130	FP- 5’AATTCGAATTCATGTCGACGCCGAGAGCGGC 3’
	RP-5’AATTCCTCGAGCTGCTCCGCCAACCCAACCGA 3’
pGADT7 Os_04g41680	FP-5’AATTCGAATTCATGGCGAACTCACCGACGCC 3’ RP-5’AATTCGAGCTCACAGTAAAGGTTGCCACCCG 3’
For BiFC study	
pSPYNE:Rs_MEP1	FP- 5’AATTCTCTAGAATGTTGTTCTCTGCGCTCTCTGTCCT 3’
	RP- 5’AATTCGGATCCGACGGTGATACCACGGTAAGTAGCGA 3’
pSPYCE:Os_41680	FP- 5’AATTCTCTAGAATGGCGAACTCACCGACGCCGAC 3’
	RP- 5’AATTCGGATCCACAGTAAAGGTTGCCACCCGGGTC 3’
For qRT-PCR	
RT- Os_03g30470	FP-5’CGACCGGATCGGCTTCTAC 3’
	RP-5’GGCCTCTGGCTGTAGCAAT 3’
RT- Os_11g47600	FP- 5’CTACTGGACCGACCTCTCCG 3’
	RP- 5’GAGGACGGGGATGTTCTTGG 3’
RT- Os_02g39330	FP- 5’GTGGCTACCCTTCCTTCGG 3’
	RP- 5’TTATGGTCTCGTGGTTGGCG 3’
RT-Os_10g28080	FP- 5’CGGGGTTGTTCATCTGGTCA 3’
	RP- 5’TCCTGAGCCTTGGTCTCGTA 3’
RT-Os_06g51060	FP- 5’CTACTGTGTCCAGAGCTCGC 3’
	RP- 5’CGGGCCGTAGTTGTAGTTGT 3’
RT-Os_06g51050	FP-5’CCTCCATCATATCGCCCTCG 3’
	RP-5’CGTCGTAGGTGTAGAAGCCC 3’
RT-Os_05g33130	FP-5’GCTTCTACCAGCGCTACTGT 3’
	RP-5’TGAACGGCCTCTGGTTGTAG 3’
RT-Os_04g41680	FP-5’AACTACAACTACGGGCCTGC 3’
	RP-5’GCCGTCTTGAAGGAGATCGT 3’
RT-Os_11g47500	FP-5’CTTGACGGGGAAGAACGACA 3’
	RP-5’TCCTCCGTACGTATCCGTGT 3’
RT-OS_18S	FP-5’CTACGTCCCTGCCCTTTGTACA 3’
	RP-5’ACACTTCACCGGACCATTCAA 3’
Sl-Actin	FP- 5’GCTCCACGAGCTGTATTTCC 3’
	RP- 5’CCGTGCTCAATTGGGTATTT 3’
Rs_18S	FP- 5’CCCCCTGTGCACTTGTGAG 3’

	RP- 5’ATCGCATTTCGCTGCGTTC 3’
RT- Rs_GT34	FP- 5’TAAGCTATCCCGCCGACTTC 3’
	RP- 5’CGCTTGCATCCCTTGACTCT 3’
RT- Rs_MEP1	FP- 5’CACTCACCCACGAAGTTGGA 3’
	RP- 5’GGGTGTCGCTAACGGAATCA 3’
RT- Rs_ABC3	FP- 5’CTCGAGCGTTTTGCCACCTA 3’
	RP- 5’TAGGCTGTGAACGGCATGAA 3’
RT- Rs_ GzZC236	FP- 5’GAAGCTCGCCCAAGGAATTT 3’
	RP- 5’ACAACCATTCACCCCAACAAA 3’
RT- Rs_PHO84	FP- 5’GCTGGCGTTGGTTTCTTCAC 3’
	RP- 5’ACCACCCTTGCCGTAGATAAAG 3’
RT- Rs_GAS	FP- 5’GCCGTTCTCGCCCTTGA 3’
	RP- 5’TCGCAGGTCGCTTCCATT 3’
RT- Rs_AOX1	FP- 5’GCCTTGGCCGTTTTGAGATA 3’
	RP- 5’ATCCCAACGCGAAAGATCAT 3’
RT- Rs_SPM1	FP- 5’CGGCCATGGAACTCACACT 3’
	RP- 5’CCAGAGCCAGAGTCAGACAGAA 3’
For Secretion trap assay	
Rs_MEP1 YST	FP-5’GAATTCATGTTGTTCTCTGCGCTCTCT 3’
	RP- 5’GCGGCCGCGACGGTGATACCACGGTAAGT 3’
Rs_MEP1–SP YST	FP-5’GCGGCCGCGACGGTGATACCACGGTAAGT 3’
	RP-5’GCGGCCGCTTAGACGGTGATACCACGGTAAG 3’
For protein purification	
RS_MEP1-PET28a	FP- 5’GCGGCCGCGACGGTGATACCACGGTAAGT 3’
	RP- 5’GCGGCCGCTTAGACGGTGATACCACGGTAAG 3’
For RNAi constructs	
Rs_MEP1 RNAi Sense	FP- 5’CCATGGTCTAGATGTTCTCTGCGCTCTCTGTC 3’
	RP- 5’CCGCGGAGAGTTGAACCAGTTCGCGT 3’
Rs_MEP1 RNAi Antisense	FP- 5’GTCGACAGAGTTGAACCAGTTCGCGT 3’
	RP- 5’GAGCTCTGTTCTCTGCGCTCTCTGTC 3’
RT- Rs_MEP1dsRNA	FP- 5’TAATACGACTCACTATAGGGAGATGTTCTCTGCGCTCTCTGTC 3’
	RP- 5’TAATACGACTCACTATAGGGAGAAGAGTTGAACCAGTTCGCGT 3’
	For transient overexpression
Pcam1302-Os_04g41680	FP- 5’GGATCCATGAGAGCGCTCGCTGTGG 3’
	RP- 5’AAGCTTGGAGCCGAAGGGCCTCTGG 3’
Pcam1302-Rs_MEP1	FP- 5’CCATGGATGTTGTTCTCTGCGCTCTCTGTCCTTG 3’
	RP- 5’ACTAGTGACGGTGATACCACGGTAAGTAGCGATTT 3’

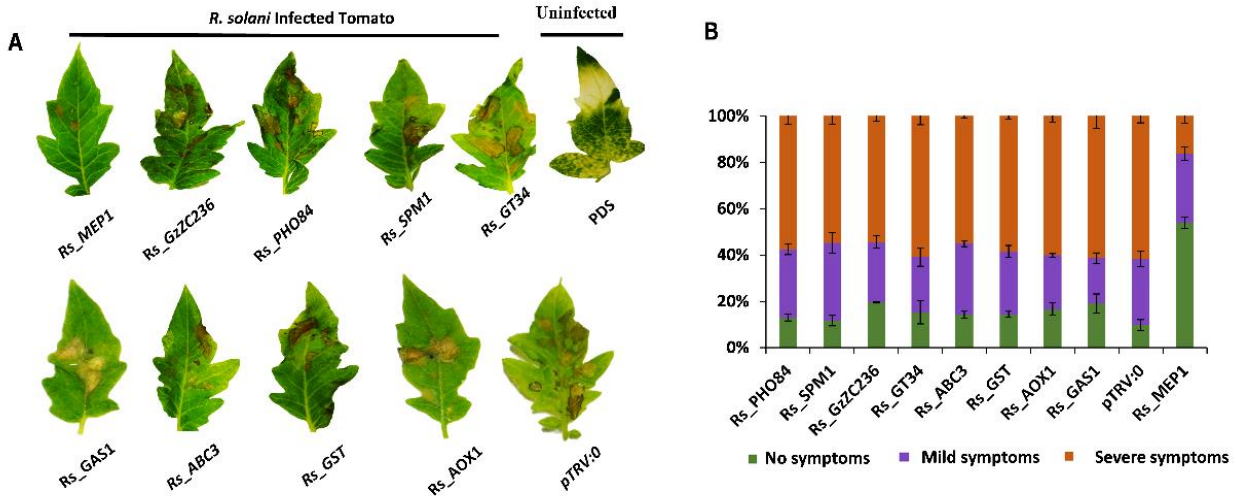

Supplementary Figure 1. Disease severity in *R. solani*-infected HIGS tomato lines for selected candidate pathogenicity determinants. **A.** Disease symptoms in HIGS plants, at 3 dpi. The photobleaching phenotype induced by silencing PDS was used as a positive control. pTRV:0 was used as vector control. *Rs_GT34* was used as a negative control. **B**. Disease index showing the percentage of leaves with no symptoms (visible necrotic symptoms not observed), mild (localized necrotic spots, <30% of infected region of the leaves showing necrotic lesions), and severe symptoms (total necrosis with coalescence of several necrotic spots, >30% of infected region of the leaves showing necrotic lesions). The graph shows the mean ± standard error of three biological replicates.

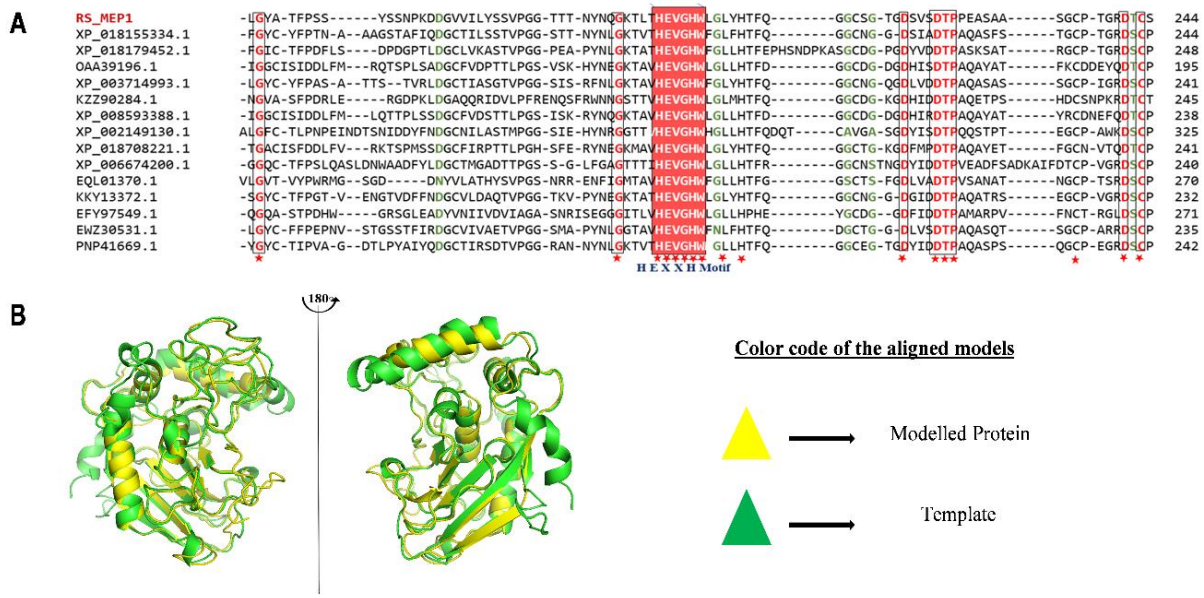

Supplementary Figure 2. Domain architecture of Rs_MEP1. **A.** Multiple sequence alignment of Metalloproteases from diverse pathogenic fungi. The conserved catalytic site HEXXH is highlighted. XP_018155334.1: *Colletotrichum higginsianum*, EWZ30531.1: *Fusarium oxysporum*, XP_018179452.1: *Purpureocillium lilacinum*, OAA39196.1: *Beauveria brongniartii*, XP_003714993.1: *Pyricularia oryzae*, KZZ90284.1: *Moelleriella libera*, XP_008593388.1: *Beauveria bassiana*, XP_002149130.1: *Talaromyces marneffei*, XP_018708221.1: *Cordyceps fumosorosea*, XP_006674200.1: *Cordyceps militaris*, EQL01370.1: *Ophiocordyceps sinensis*, KKY13372.1: *Diplodia seriata*, EFY97549.1: *Metarhizium robertsii*, PNP41669.1: *Trichoderma gamsii*. **B.** Three-dimensional (3D) structural model of Rs_MEP1 using I-TASSER, showing structural analogy with a promirolysin protein (6R7V). The yellow and green colors represent Rs_MEP1 and promirolysin, respectively.

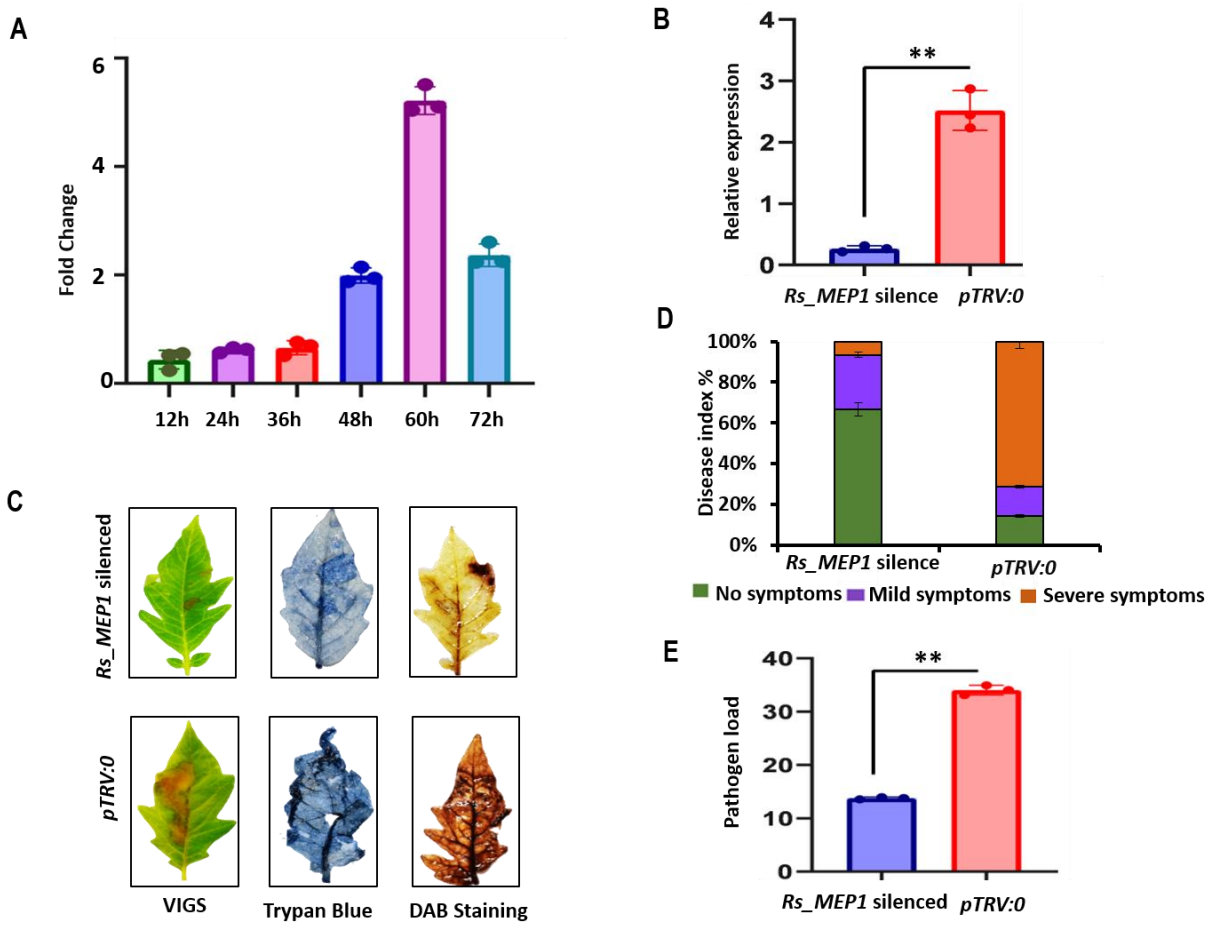

Supplementary Figure 3. *Rs_MEP1* is an important pathogenicity determinant of *R. solani*. **A.** qRT-PCR-based expression analysis of *Rs_MEP1* in the infected tomato leaves, at different time points. **B.** qRT-PCR-based expression analysis, showing effective silencing of *Rs_MEP1* in the HIGS plants. The expression was normalized using *R. solani 18S rRNA*. **C.** The disease symptoms, trypan blue staining showing cell death, and DAB staining reflecting enhanced ROS accumulation, in the infected leaves, at 3 dpi. **D.** Disease index showing the percentage of leaves with no symptoms, mild symptoms, and severe symptoms, and **E.** Pathogen load in *Rs_MEP1* silenced HIGS plants, compared to vector control plants, at 3 dpi. The pathogen load was estimated as the abundance of 18S rRNA from *R. solani*, normalized to the tomato actin gene. The graph shows the mean ± standard error across three biological replicates. (**) indicates a significant difference between vector control and HIGS lines, at $p \leq 0.001$.

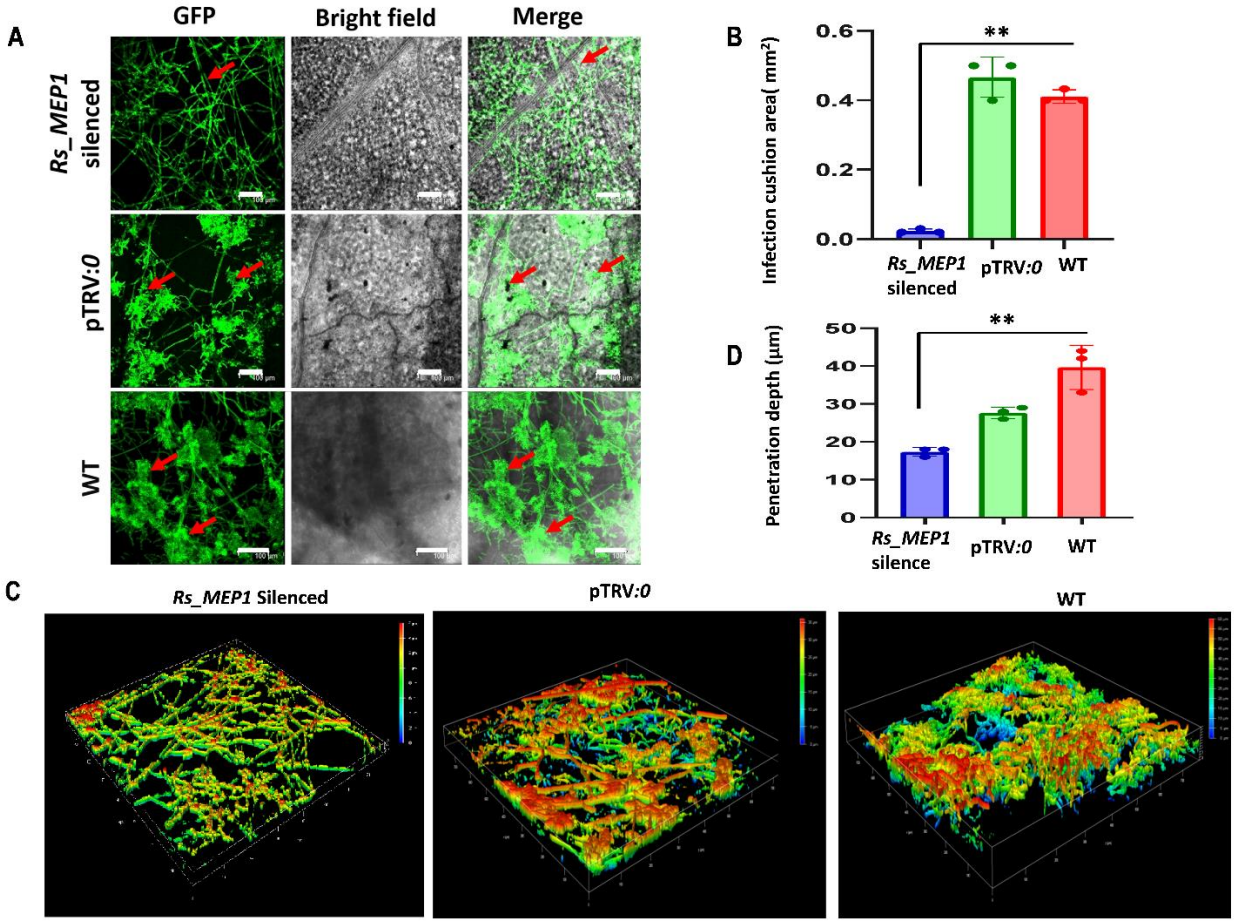

Supplementary Figure 4. Infection cushion formation and depth of host penetration are compromised in *Rs_MEP1* HIGS tomato plants. **A**. Confocal microscopic analysis, showing the formation of infection cushions is reduced in HIGS plants (TRV-*Rs_MEP1*-infiltrated), compared to wild-type (WT) and vector control (pTRV:0-infiltrated) plants. The red arrow indicates the infection cushions. Scale: 100µm. **B**. Infection cushion area in the infected leaves. **C**. The penetration depth and **D**. Topological overview of *R. solani* penetration in infected leaves. The index bar in the z-axis represents the depth of penetration. The graphs show the mean ± standard error across three biological replicates. (**) indicates a significant difference at $p \leq 0.001$ between vector control and HIGS lines.

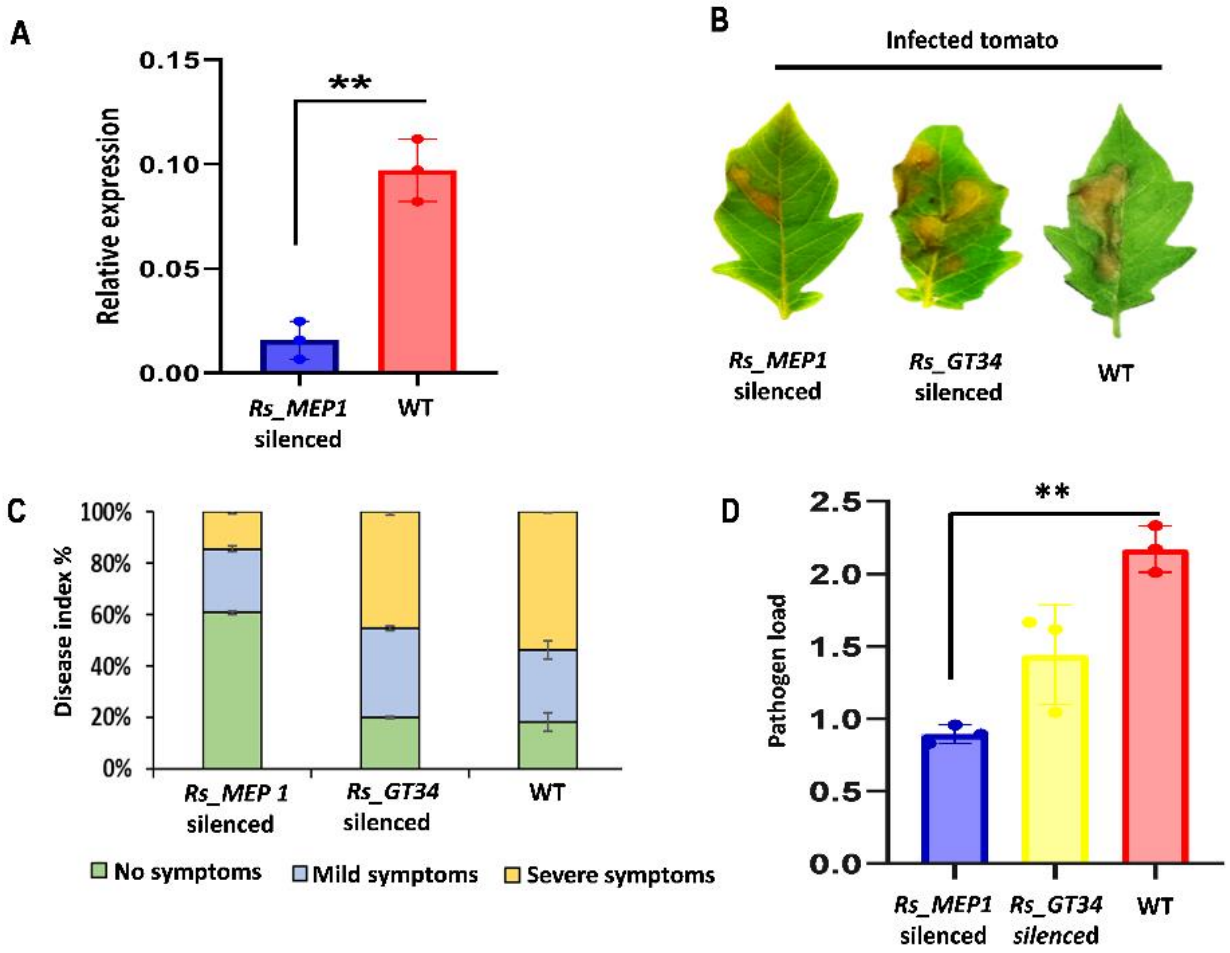

Supplementary Figure 5. dsRNA-mediated silencing of *Rs_MEP1* significantly compromises the pathogenesis of *R. solani* in tomato. **A.** qRT-PCR-based expression analysis of *Rs_MEP1* in dsRNA-treated (*Rs*_MEP1-silenced) and buffer-treated (WT) *R. solani* sclerotia. *R. solani 18S rRNA* was used as an endogenous control to calculate the relative expression of target genes. **B.** Disease symptoms in tomato, infected with *Rs_MEP1*-silenced, *Rs_GT34*-silenced, and buffer-treated *R. solani,* at 3 dpi. **C.** Disease severity index reflecting the percentage of leaves with no symptoms (visible necrotic symptoms not observed), mild (localized necrotic spots, <30% of infected region of the leaves showing necrotic lesions), and severe symptoms (total necrosis with coalescence of several necrotic spots, >30% of infected region of the leaves showing necrotic lesions). **D.** Pathogen load in the infected tomato leaves. The tomato actin gene of tomato was used as an endogenous control. The graph shows the mean ± standard error of three biological replicates. (**) indicates a significant difference at $p \leq 0.001$.

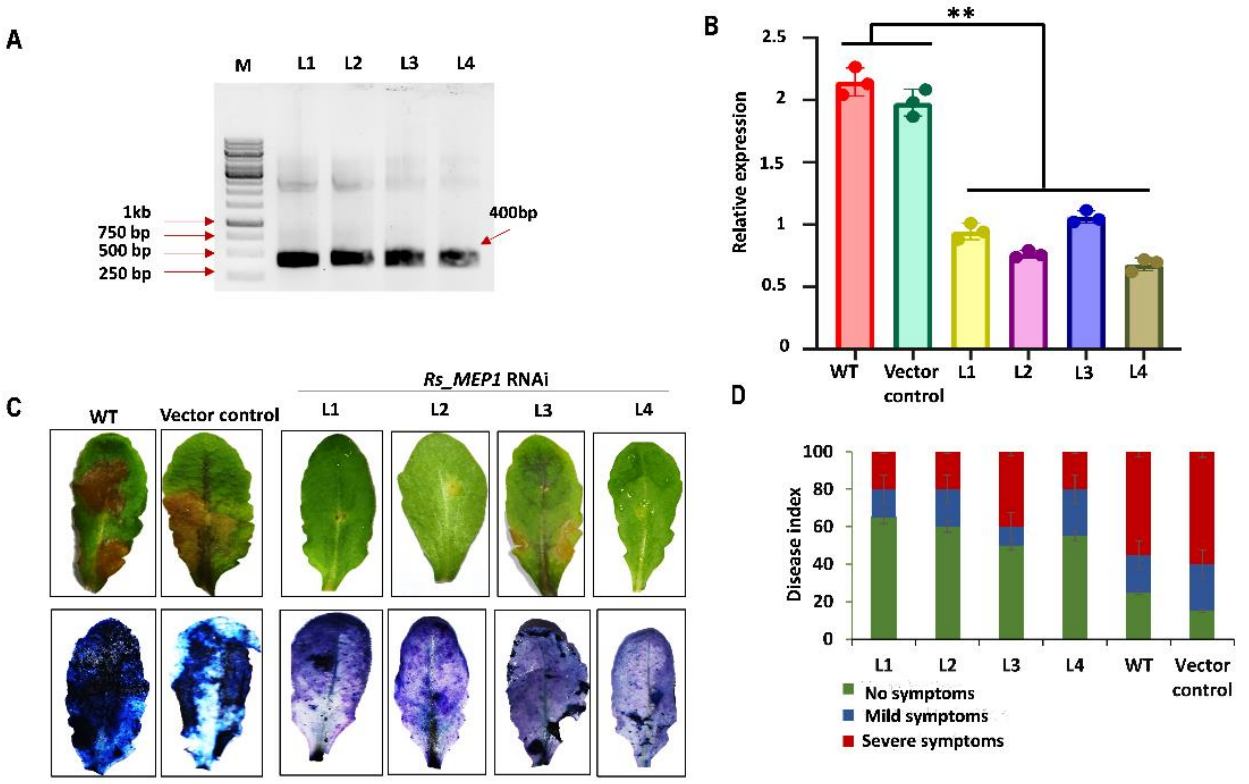

Supplementary Figure 6. Characterization of *Rs_MEP1* RNAi lines in *Arabidopsis*. **A.** PCR-based confirmation of *Arabidopsis* RNAi lines using intron-specific primers (400 bp). **B.** qRT-PCR expression analysis of *Rs_MEP1* in *Arabidopsis* lines. The relative expression was estimated using *Actin* gene of *A. thaliana* as an endogenous control. **C.** Disease symptoms (upper panel) and trypan blue staining of the infected leaves, reflecting cell death (lower panel). **D.** Percentage disease severity index in different lines, upon *R. solani* infection at 4 dpi. No symptoms (visible necrotic symptoms not observed), mild (localized necrotic spots, <30% of infected region of the leaves showing necrotic lesions), and severe symptoms (total necrosis with coalescence of several necrotic spots, >30% of infected region of the leaves showing necrotic lesions). The graph shows the mean ± standard error across three biological replicates. (**) indicate a significant difference at $p \leq 0.001$.